

ACKNOWLEDGMENTS

I would like to thank my advisor, Dr. Garry R. Buettner, for his constant support, excellent guidance, and a positive outlook on science and life.

I would like to thank my committee members, Drs. Larry W. Oberley, Mike E. C. Robbins, Frederick E. Domann, Bradley E. Britigan, and Stephen L. Hempel, for their critical evaluation, helpful suggestions, and precious time.

I would also like to thank my EPR 'buddies', Sean Martin, Hong Wang, Brett Wagner, Eric Kelley, and Drs. Freya Schafer, Mike McCormick, David Hall, Sujatha Venkataraman, Yuanxia O'Malley who helped me in many ways to complete my project.

Especially, I want to thank my wife, Xiaohong Jiang, and my daughters, Ying Qian and Jessica Qian. Without their whole hearted love, support, and sacrifice, I would not have finished this work.

TABLE OF CONTENTS

	Page
LIST OF TABLES	v
LIST OF FIGURES	vi
LIST OF SCHEMES	iviii
LIST OF ABBREVIATIONS.....	ix
 CHAPTER	
I. INTRODUCTION.....	1
Lipid Peroxidation.....	2
Photo-Oxidation	3
Lipid-Derived Radicals and EPR Detection.....	5
Short Lifetime Limits the Detection of L_d^\bullet	9
Combination of EPR and Extraction.....	10
Research Summary.....	10
II. MATERIALS AND METHODS	13
Materials	13
Buffer Solutions	13
The Ascorbate Test	13
Spin Traps	14
Fe^{2+} and Cu^{2+} Solutions	14
Chelators	14
Docosahexaenoic Acid (DHA)	15
Photofrin.....	15
Low-Density Lipoprotein (LDL).....	15
Suspension Cells	15
Adhesive Cells	16
Methods	17
The Order of Addition.....	17
EPR Measurement.....	17
Ethyl Acetate Extraction.....	18
Folch Extraction for LDL and K-562 Cells	18
Folch Extraction for MCF-7 Cells.....	18
Photofrin/Light Treatment	18
Oxygen Monitor	19
Anaerobic Suspension.....	19

III.	EPR STUDY OF DHA PEROXIDATION.....	20
	DMPO in DHA Suspension Study.....	21
	DHA Oxidation in Anaerobic Suspension.....	24
	DHA Oxidation in Open Suspension.....	26
	DHA Oxidation in Closed (Air-Saturated) Suspension.....	32
	Summary of DMPO in DHA Suspension Study.....	39
	DMPO Study and E.A. Extraction.....	40
	Location of DMPO and the DMPO Adducts After Extraction....	42
	Extraction Increases Stability of DMPO Spin Adducts.....	47
	Identification of DMPO Adduct Post-Extraction.....	47
	Radical Profile Determined by EPR-Extraction.....	58
	Summary of EPR-Extraction.....	61
	DEPMPO in a DHA Study.....	62
	DEPMPO Study and E.A. Extraction.....	63
	Define the Lipid Peroxyl-Type Radicals.....	71
	Summary of DEPMPO Study.....	75
IV.	EPR STUDY OF LIPID PEROXIDATIONS IN CELLS AND LDL	
	79
	Lipid Peroxidation in K-562 Cells.....	80
	EPR study in Cell Suspension.....	80
	EPR-Extraction and K-562 Oxidation.....	82
	Summary of K-562 Cell Study.....	86
	Lipid Peroxidation in MCF-7 Cells.....	87
	EPR-Extraction and MCF-7 Cell Oxidation.....	87
	Summary of MCF-7 Cell Study.....	91
	Low-Density Lipoprotein Oxidation.....	91
	EPR-Extraction and LDL Oxidation.....	91
	Summary of LDL Study.....	92
V.	FUTURE DIRECTIONS.....	95
	HPLC and MS.....	96
	REFERENCES.....	99

LIST OF TABLES

Table		Page
1.	The properties of nitroso and nitrono compounds.....	7
2.	Extraction improves the identification of DMPO spin adducts.....	41
3.	Different oxidized status of DHA causes different O ₂ depletion.....	72

LIST OF FIGURES

Figure		Page
1.	EPR spectra of DMPO/L _d • formed from the Fe ²⁺ -mediated DHA oxidation in aerobic suspension.....	22
2.	EPR spectra of DMPO/L _d • formed from the Fe ²⁺ -mediated DHA oxidation in anaerobic suspension.....	25
3.	The profile of DMPO/L _d • detected by EPR in Fe ²⁺ -mediated DHA oxidation in an anaerobic PB suspension.....	27
4.	The profile of DMPO/L _d • detected by EPR in Fe ²⁺ -mediated DHA oxidation in open suspension.....	28
5.	EPR spectra of DMPO/L _d • formed during Fe ²⁺ -mediated DHA oxidation.....	29
6.	The profile of DMPO/L _d • detected by EPR in Fe ²⁺ -mediated DHA oxidation in closed, air-saturated suspension.....	33
7.	The comparison of all adduct yields formed from three different oxygen profile, e.g. N ₂ -, air-saturated and opened systems.....	34
8.	O ₂ depletion experiment in Fe ²⁺ -mediated DHA oxidation.....	37
9.	EPR spectra of DMPO/L _d • formed from Fe ²⁺ -mediated DHA oxidation in closed (air-saturated) suspension.....	38
10.	DMPO remains in the aqueous phase after E.A. extraction.....	43
11.	DMPO remains in the aqueous phase after CHCl ₃ extraction.....	44
12.	The distribution of DMPO adduct of •CH ₃ , •OCH ₃ , and •OOCH ₃ after E.A. extraction.....	45
13.	Extraction with E.A. increases the lifetime of DMPO adducts observed during DHA lipid peroxidation.....	48
14.	Two DMPO adducts are observable in the organic phase (E.A.) after extraction in DHA-peroxidizing system.....	49
15.	At least three DMPO adducts are clearly observed in the aqueous phase post-extraction in the DHA-peroxidizing system.....	51
16.	Comparison of DMPO adduct yield observed in the aqueous phase before and after E.A. extraction.....	54

17.	The distribution of DMPO/ [•] OH and DMPO/ [•] OOH after E.A. extraction	56
18.	The profile of lipid-chain radical adduct detected by an EPR-extraction.	59
19.	EPR spectra of DEPMPO/L _d [•] formed by Fe ²⁺ -mediated DHA oxidation	64
20.	Extraction with E.A. increases the lifetime of DEPMPO adducts observed during DHA lipid peroxidation.....	66
21.	The distribution of DEPMPO/ [•] OH and DEPMPO/ [•] OOH during our extraction procedure	69
22.	DEPMPO adducts observed during DHA lipid peroxidation.....	73
23.	The relation of species C, e.g. peroxy-type radical, and [DEPMPO].....	77
24.	EPR spectra of DEPMPO/L _d [•] and DMPO/L _d [•] formed from Photofrin-mediated membrane lipid peroxidation in K-562 cells.....	83
25.	Lipid radicals can be trapped by DMPO from intact K-562 cells using the combination of EPR and Folch extraction.....	85
26.	Lipid-derived free radicals are generated from MCF-7 cells following Photofrin/light treatment.....	89
27.	Radical yields from MCF-7 cells and their L-PhGPx transfectants.....	90
28.	Lipid radical production from LDL oxidation	93

LIST OF SCHEMES

Scheme		Page
1.	Overview of the chemistry of the formation of lipid-derived radicals (L_d^\bullet) produced during lipid peroxidation in the presence of ferrous iron.....	4
2.	Overview of the formation of lipid-derived radicals produced during lipid peroxidation and their EPR spin trapping reactions	8
3.	Outline of how the different components of the lipid-spin trapping system, partition after extraction of the complete reaction system using an organic solvent.....	11
4.	Outline of mechanism lipid peroxidation of DHA	76
5.	Proposed mechanism of Photofrin-mediated cellular lipid peroxidation .	81
6.	The schematic diagram of HPLC and MS	97

LIST OF ABBREVIATIONS

a^H :	hyperfine constant from hydrogen atom
a^N :	hyperfine constant from nitrogen atom
a^P :	hyperfine constant from phosphorus atom
A.U.:	arbitrary units
DEPMPO:	5-diethoxyphosphoryl-5-methyl-pyrroline-N-oxide
DHA:	docosahexaenoic acid
DMPO:	5,5-dimethyl-pyrroline-1-oxide
DTPA:	diethylenetriaminepentaacetic acid
E.A.:	ethyl acetate
EDTA:	ethylenediaminetetraacetic acid
EPR:	electron paramagnetic resonance
FBS:	fetal bovine serum
GSH:	reduced glutathione
GSSG:	oxidized glutathione
HPLC:	high performance liquid chromatography
HX:	hypoxanthine
$L\cdot$:	lipid alkyl radical
$L_d\cdot$:	lipid-derived radical, a general representation for all the radicals that can be produced in lipid peroxidation
LDL:	low-density lipoprotein
LH:	unsaturated lipid
$LO\cdot$:	lipid alkoxy radical

LOO [•] :	lipid peroxy radical
LOOH:	lipid hydroperoxide
K-562:	human chronic myelogenous leukemia cells (suspension cells)
MCF-7:	human breast adenocarcinoma cells (adherent cells)
MEM:	minimal essential medium
MS	mass spectrometry
¹ O ₂ :	singlet oxygen
[O ₂] _{ss} :	steady-state concentration of O ₂
OL [•] :	lipid epoxyallylic radical
OLOO [•] :	lipid epoxyperoxy radical
R [•] :	small molecular weight carbon-centered radical
PB:	potassium phosphate buffer solution
PBS:	potassium phosphate buffer saline
PDT:	photodynamic therapy
PhGPx:	phospholipid hydroperoxide glutathione peroxidase
POBN:	α-[4-pyridyl-1-oxide]-N- <i>tert</i> -butyl nitron
PUFA:	polyunsaturated fatty acid
S:	ground state of sensitizer
¹ S [*] :	singlet excited state of sensitizer
³ S [*] :	triplet excited state of sensitizer
SH [•] :	semireduced sensitizer radical
SA:	spin adduct
ST:	spin trap
X [•] :	oxidizing species
XO:	xanthine oxidase

CHAPTER I

INTRODUCTION

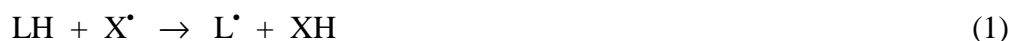
Determination of the radical species formed during lipid peroxidation is essential for the complete understanding of the free radical mechanisms by which cells are damaged and killed. In free radical-mediated lipid peroxidation, many different kinds of lipid-derived radicals (L_d^\bullet) can be produced [Marnett LJ, 1996; Wilcox AL, 1993; Girotti AW, 1985; Gardner HW, 1989]. They are carbon-centered radicals (lipid alkyl L^\bullet , β -scission alkyl R^\bullet , epoxyallylic OL^\bullet) and oxygen-centered radicals (alkoxyl LO^\bullet/RO^\bullet , peroxy LOO^\bullet/ROO^\bullet , and epoxyperoxy $OLOO^\bullet$). Using α -[4-pyridyl-1-oxide]-*N*-*tert*-butyl nitron (POBN), we have been successful in the EPR spin trapping of carbon-centered radicals from intact cells during lipid peroxidation [Wagner BA, 1993; 1994; Buettner GR, 1993; Qian SY, 1999]. POBN adduct formation during cellular lipid peroxidation correlates well with cell membrane damage as measured by the TBAR assay and Trypan blue dye exclusion [Kelley EE, 1997; Wagner BA, 1998; Schafer FQ, 1999].

However, POBN is only an efficient spin trap for carbon-centered radicals (R^\bullet) derived from β -scission of lipid alkoxyl radicals (LO^\bullet) during lipid peroxidation. It is believed that these carbon-centered radicals are less cytotoxic than the oxygen-centered radicals due to their lower reactivity and their location [Marnett LJ, 1996; Wilcox AL, 1993]. Thus, it is important to develop methods to detect oxygen-centered lipid radicals such as lipid alkoxyl (LO^\bullet) and lipid peroxy radicals ($OLOO^\bullet$ or LOO^\bullet) in order to understand their detrimental roles in lipid peroxidation.

In this research, I have applied extraction techniques in conjunction with EPR spin trapping in an attempt to observe the variety of lipid-derived radicals that arise during the oxidation of polyunsaturated fatty acids (PUFA), low-density lipoprotein (LDL), and cell (K-562, MCF-7) membranes.

Lipid Peroxidation

Lipid peroxidation is a free radical event consisting of three distinct steps [Girotti AW, 1985; Gardner HW, 1989]: initiation, propagation, and termination. The initiation step of lipid peroxidation can be expressed by the following reaction:



Where LH represents the lipid, and X^{\bullet} represents a highly oxidizing species such as hydroxyl radical, ferryl or perferryl species, or the triplet excited state of a photosensitizer. In reaction 1, a weakly bonded hydrogen atom is abstracted from LH by X^{\bullet} , converting the lipid to a lipid alkyl radical (L^{\bullet}).

In the propagation step, L^{\bullet} rapidly reacts with O_2 to form lipid peroxy radical (LOO^{\bullet}) (reaction 2). And then LOO^{\bullet} abstracts a hydrogen atom from another lipid to form a lipid hydroperoxide (LOOH) and a new L^{\bullet} (reaction 3).



Reactions 2 and 3 comprise the propagation cycle of lipid peroxidation. If sufficient O_2 and lipids are available, this cycle will continue, resulting in the continuation of lipid peroxidation.

When ferrous iron is available during the propagation step, lipid alkoxy (LO^{\bullet}) will form *via* the Fenton-type reaction (4).



Like LOO^\bullet in reaction 3 and Scheme 1, LO^\bullet is also usually believed to abstract a hydrogen atom from lipid chains, thereby initiating an additional radical chain and propagating lipid peroxidation. However, due to its very short lifetime, LO^\bullet may prefer to rapidly rearrange forming epoxyallylic radicals (OL^\bullet) that further react with oxygen to form epoxyperoxyl radicals (OLOO^\bullet), a longer-lived radical [Marnett LJ, 1996; Wilcox AL, 1993]. See Scheme 1. These longer-lived species are currently thought to be the major propagating species in lipid peroxidation.

Termination step occurs when L^\bullet_d produced in the initiation and the propagation steps react with each other to form nonradical products (reactions 5-9).

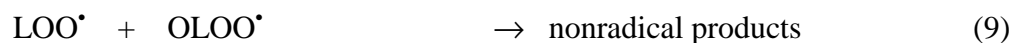
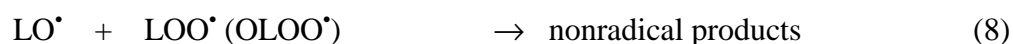
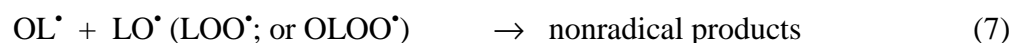
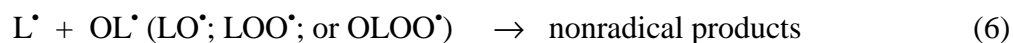
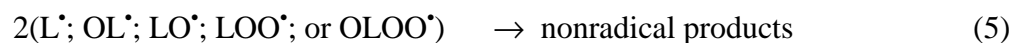


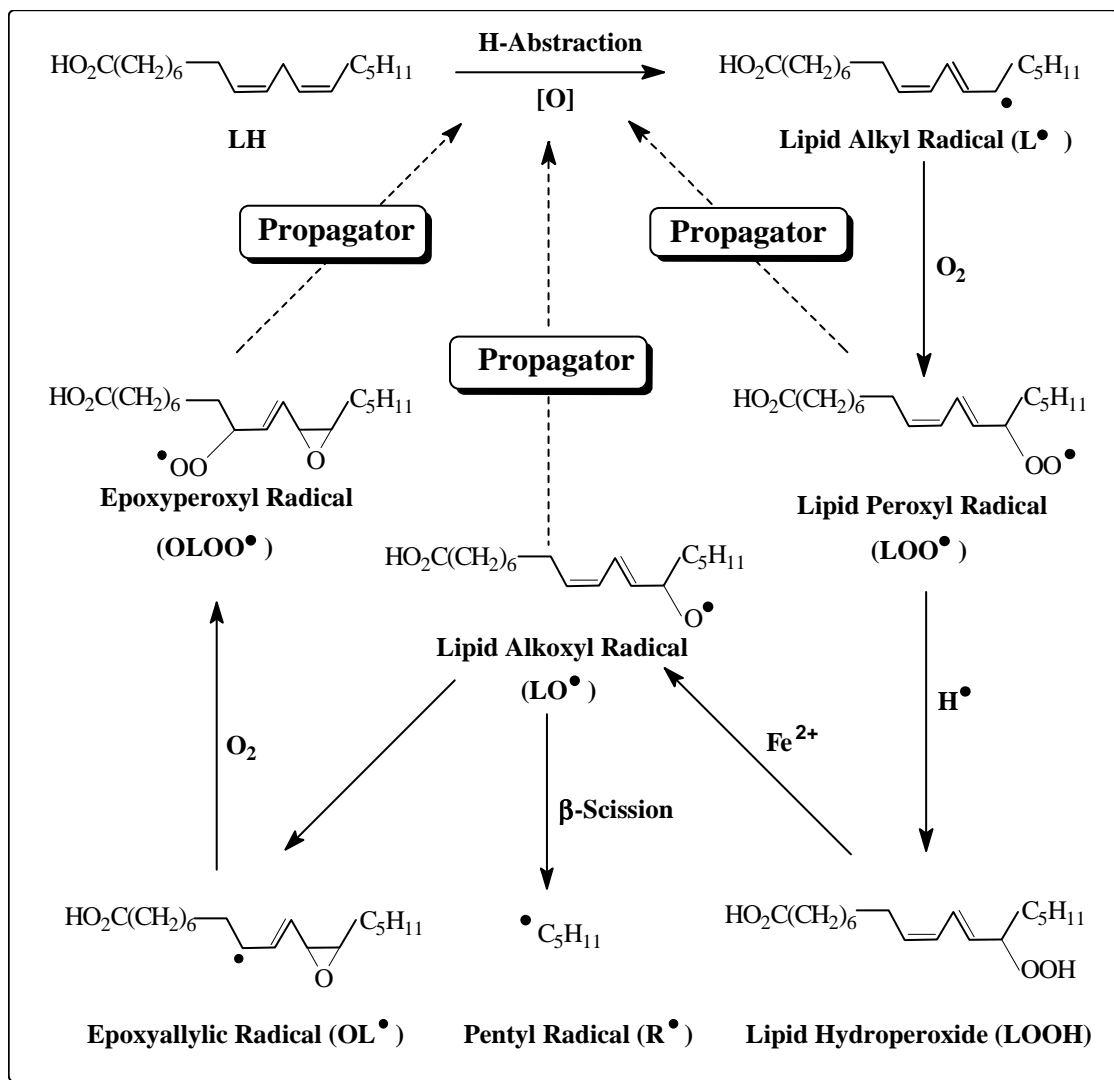
Photo-Oxidation

Photosensitizer-mediated lipid peroxidation is perhaps the most interesting research field because of the diversity in reactions and mechanisms. During photo-oxidation, a sensitizer absorbs a photon and is thereby elevated from its ground state (S) to a singlet excited state ($^1\text{S}^*$), which can then produce the energetic and longer-lived triplet state ($^3\text{S}^*$) species. See reaction 10.



There are two pathways, Type I and Type II, that can induce photo-mediated lipid peroxidation.

In type I, $^3\text{S}^*$ reacts with the allylic hydrogen atoms of PUFAs producing a

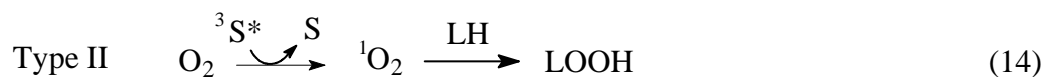


Scheme 1. Overview of the chemistry of the formation of lipid-derived radicals ($L_d\cdot$) produced during lipid peroxidation in the presence of ferrous iron. This scheme shows some of the radical species formed in the peroxidation of linoleic acid. Three different propagating species are shown. It is currently thought that $OLOO\cdot$ may be the major propagating species in this type of system [Marnett LJ, 1996; Wilcox AL, 1993].

semireduced sensitizer radical (SH^\bullet) and L^\bullet which then reacts with oxygen thereby entering the propagation step of lipid peroxidation (reaction 11). Additionally, SH^\bullet may reduce oxygen to superoxide ($\text{O}_2^{\bullet-}$, reaction 12). The disproportionation of $\text{O}_2^{\bullet-}$ produces H_2O_2 , which reacts with $\text{O}_2^{\bullet-}$ *via* Haber-Weiss reaction (reaction 13) giving HO^\bullet that induces additional oxidation processes.



In a type II process, energy transfers from the triplet state sensitizer to ground state O_2 producing excited state singlet oxygen ($^1\text{O}_2$). Singlet oxygen can covalently add to unsaturated lipids to form LOOHs *via* a non-radical mechanism (reaction 14).



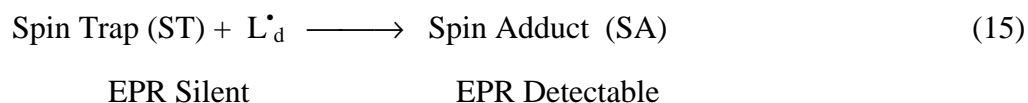
These hydroperoxides can induce radical chain oxidations upon addition of ferrous iron due to the formation of LO^\bullet , a propagator of lipid peroxidation (Scheme 1).

In our Photofrin-mediated cell membrane oxidations, the membrane lipid hydroperoxides were produced from Photofrin/light treatment, predominantly through the Type II pathway [Jori G, 1980; Wilkinso F, 1981]. If more hydroperoxides were produced in cell membranes by Photofrin-treatment, cells would be more efficiently killed by membrane radical oxidations.

Lipid-Derived Radicals and EPR Detection

Determination of what kind of radical and the amount of radical produced is a starting point to understand the mechanism by which free radicals damage cells. As

shown in Scheme 1, there are different types of L_d^\bullet formed during lipid peroxidation. Unfortunately, these radicals are all extremely difficult to detect directly by EPR due to their very short lifetimes. Thus, to study L_d^\bullet , spin-trapping was used to convert these short-lived radicals to more stable compounds, spin adducts. See reaction 15. The spin adduct can be readily detected by EPR and may have hyperfine splitting constants that reflect the nature and structure of the L_d^\bullet .



There are two categories of compounds commonly used as spin traps: nitroso and nitron compounds. The properties of some of those compounds are listed in Table 1. For the purpose of this research, nitrones seem more useful because they react less readily with unoxidized lipids than do nitroso compounds [Feix JB, 1989; Mason RP, 1980]. In addition, they can trap both carbon-centered and oxygen-centered radicals [Buettner GR, 1987]. In principle, L_d^\bullet can be detected by EPR spin trapping as shown as Scheme 2. However, because of the complicated pathway of lipid peroxidation, failure to consider the kinetics of the spin trapping reaction and spin adduct termination, as well as failure to consider the oxygen-broadening effect can lead to artifacts or misassignment of EPR spectra.

We have been successful in the EPR detection of the β -scission radicals formed in cells exposed to Photofrin and light using POBN as a spin trap [Buettner GR, 1993; Wagner BA, 1993, 1994; Qian SY, 1999].

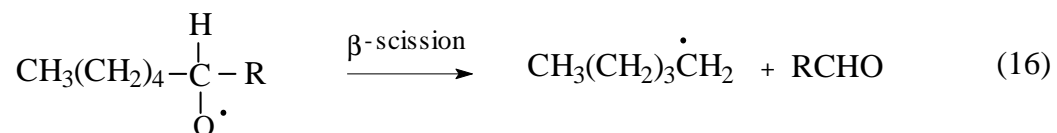
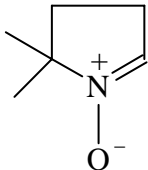
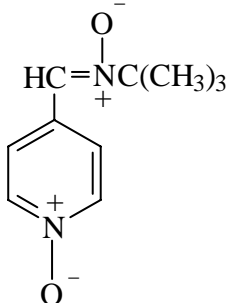
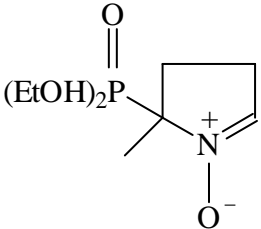
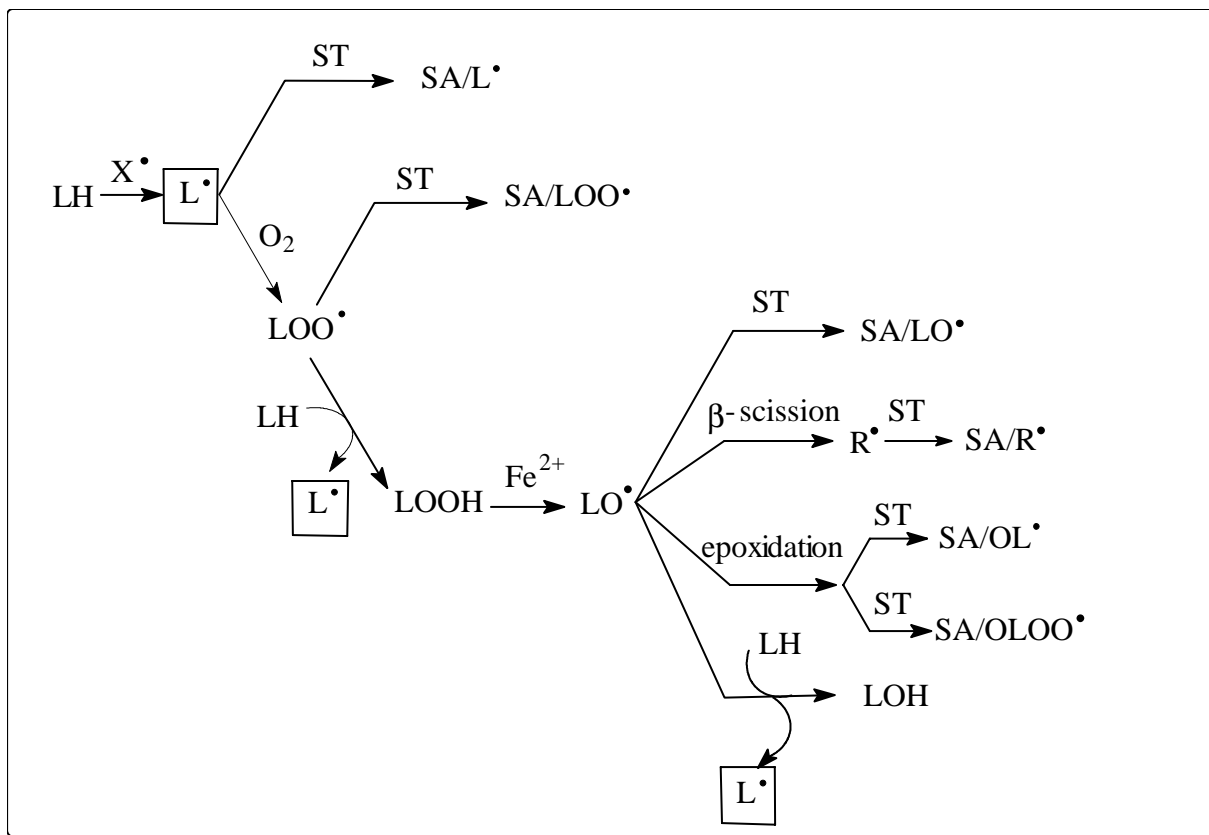


Table 1. The properties of nitroso and nitron compounds

Structure	Name	Radicals trapped	Reacts with unoxidized PUFA
	DMPO nitron	carbon-centered and oxygen-centered radicals	No
	POBN nitron	carbon-centered radicals	No
	DEPMPO nitron	carbon-centered and oxygen-centered radicals	No
(CH ₃) ₃ C-NO	MNP nitroso	carbon-centered	Yes [Mason RP, 1980]



Scheme 2. Overview of the formation of lipid-derived radicals produced during lipid peroxidation and their EPR spin trapping reactions. Here, L represents lipid; X• represents oxidizing species; ST represents spin trap; SA represents spin adduct; and R• represents small fragment carbon-centered radical.

Radical formation correlates with cell damage (TBARs) or Photofrin phototoxicity (trypan blue dye exclusion) [Kelley EE, 1997; Wagner BA, 1998; Schafer FQ, 1999].

However, POBN is only an efficient spin trap for carbon-centered radicals derived from β -scission of lipid alkoxyl radicals but is not efficient for oxygen-centered radicals. It is believed that the β -scission, carbon-centered radicals are less cytotoxic than the oxygen-centered lipid radicals due to their lower reactivity and their location [Marnett LJ, 1996; Wilcox AL, 1993]. Thus, it is important to develop methods to detect oxygen-centered lipid radicals such as lipid alkoxyl (LO^{\bullet}) and lipid peroxy radicals ($OLOO^{\bullet}$ or LOO^{\bullet}) in order to determine their detrimental role in lipid peroxidation. Using EPR with DMPO spin trapping, Chamulitrat *et al.* and Davies *et al.* detected oxygen-centered lipid radicals in enzyme-dependent hydroperoxide reactions [Chamulitrat W, 1991; Davies MJ, 1987; 1988]; Schaich *et al.* detected these types of radicals with organic extraction [Schaich KM, 1990; Kalyanaraman B, 1984; Chamulitrat W, 1992]. To our knowledge, however, there is no report on the successful EPR detection of oxygen-centered lipid radicals produced during cell membrane lipid peroxidation.

Short Lifetime Limits the Detection of L_d^{\bullet}

The free radicals produced during lipid peroxidation can undergo various termination reactions (reaction 19, *e.g.* reaction 5-9) that compete with the spin trapping reaction (reaction 18). However, these radicals can also react with the DMPO spin adducts that have been formed (reaction 20). Peroxyl radicals react with nitroxides with rate constants of 10^4 - 10^5 $M^{-1}s^{-1}$, while alkyl radicals, such as the carbon-centered radicals produced during lipid peroxidation, react with nitroxides at near diffusion-controlled rates ($k > 10^{10}$ $M^{-1}s^{-1}$) [Kocherginsky N, 1995]. Thus, reaction 20 will be a significant route to the destruction of spin adducts formed during lipid peroxidation.





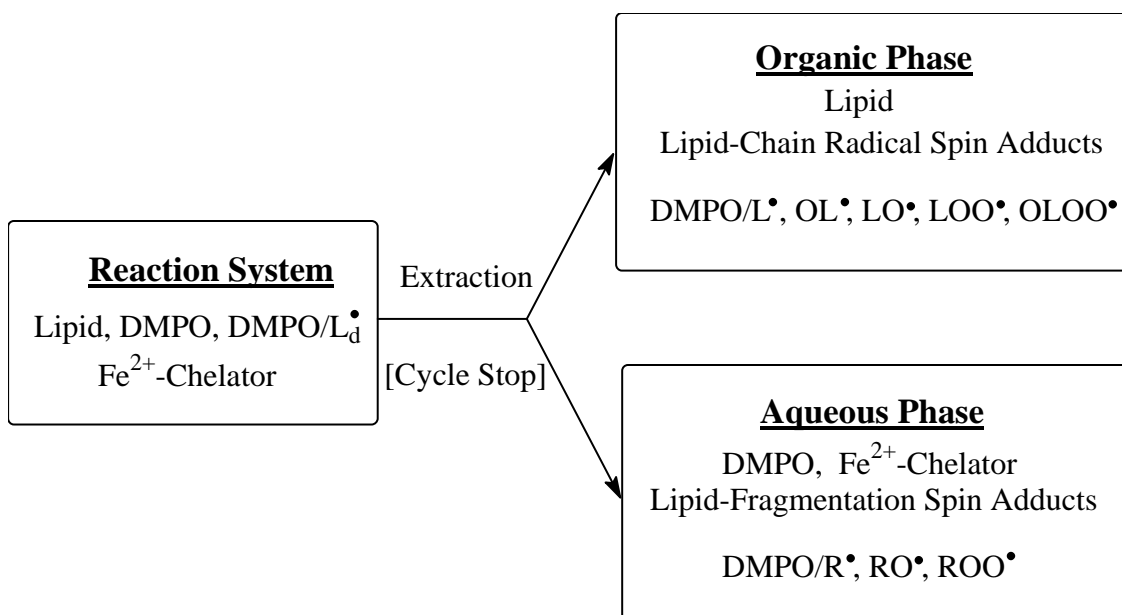
We hypothesized that the destruction of DMPO spin adducts *via* reaction 20 is the major reason the adducts have such short lifetimes and why their EPR spin trapping detection is so difficult. In a normal EPR spin trapping study of lipid peroxidation, the detection of peroxy-type radicals has always been a serious problem due to their very short lifetimes. The main goal of this research was to find a way to successfully detect these species.

Combination of EPR and Extraction

I propose that EPR spin trapping followed by extraction can stabilize the DMPO adducts. I have developed an extraction method to separate the oxidizable substrate (lipids) from the mediator of oxidation (iron), Scheme 3. Our extraction process will not only separate iron ions (oxidation mediator, in aqueous phase) from the oxidizable lipids (in organic phase), but also will dilute reactants and products. Thus, the extraction can stop or slow the lipid peroxidation cycle, and consequently slow the reactions that destroy the spin adduct (reaction 20). Applying this extraction protocol at specific time points allows the profile of lipid-derived radicals to be determined. This time profile of the radical production will allow us to better understand the dynamics of radical formation and the role of the different radicals in the lipid peroxidation.

Research Summary

My research hypothesis is that the combination of EPR spin trapping and an extraction technique allows us to stop the lipid peroxidation, thereby stabilizing the spin adducts for EPR spectral analysis and for future HPLC and MS studies. To test this hypothesis, I used ethyl acetate (E.A.) to extract the DMPO lipid radical adducts derived



Scheme 3. Outline of how the different components of the lipid-spin trapping system partition after extraction of the complete reaction system using an organic solvent, such as ethyl acetate or the Folch extraction solvent system. Here, L represents the long-chain lipid species; L_d[•] represents all the potential lipid-derived radicals that could be spin trapped by DMPO; R represents the short-chain fragmentation products that can be produced during lipid peroxidation. In our experimental protocol, the organic phase of the extraction is first evaporated to dryness using argon or nitrogen. Then nitrogen-purged ethyl acetate is used to dissolve the spin adducts for EPR examination. Using this protocol any DMPO as well as small molecular weight spin adducts (volatile), such as DMPO/HO[•], that have partitioned into the organic phase have been removed, leaving only the long chain fatty acids and long-chain radical adducts. The removal of DMPO also avoids the formation of additional spin adducts in the organic phase after extraction. The aqueous phase is observed directly.

from Fe^{2+} -mediated DHA oxidation, and used the Folch extraction ($\text{CHCl}_3/\text{CH}_3\text{OH}$) to extract DMPO lipid radical adduct from LDL and cell membrane oxidation experiments. In all experimental models, the lifetimes of the DMPO adducts of oxygen-centered lipid radical post-extraction are much longer (> 10 h) than the lifetimes of DMPO radical adducts without extraction (< 20 min). In addition, combining EPR spin trapping with an extraction process provides a way to detect different types of radical adducts in different phases. Using our extraction protocol (Scheme 3), the long-chain lipid radicals (OL^\bullet , LO^\bullet , LOO^\bullet , OLOO^\bullet) are detected mainly in the organic phase, while the small fragment radicals (R^\bullet , HO^\bullet , RO^\bullet , ROO^\bullet) are mostly present in the aqueous phase. This is important for further HPLC and MS studies where these radicals have to be separated.

CHAPTER II

MATERIALS AND METHODS

Materials

Buffer Solutions

All DHA and LDL experiments were performed in 50 mM potassium phosphate-buffer (PB, pH 7.4). All cell experiments were performed in 50 mM potassium phosphate-buffer saline (PBS, pH 7.4). The potassium dihydrogen phosphate (KH_2PO_4), dipotassium hydrogen phosphate (K_2HPO_4), and NaCl were purchased from Fisher (Fisher Scientific Co. Fair Lawn, NJ).

Adventitious metals in PB and PBS were removed by treatment of a chelating resin (sodium form, dry mesh 50-100, from Sigma, St. Louis, MO). After washing the resin with portions of PB or PBS several times to neutralize its strongly acidic or basic properties, the resin was then added to the PB or PBS using about 10 mL of resin per liter of solution. In order to achieve good chelating results, PB and PBS solutions were stirred gently for at least 12 h. A pH value of 7.4 was obtained by adding HCl or NaOH (1M, Fisher). PB and PBS solutions were ready to be used in experiments after passing the ascorbate test [Buettner GR, 1988].

The Ascorbate Test

Ascorbic acid is a diacid, with pK_a values of 4.2 and 11.6. The spontaneous oxidation of ascorbate monoanion at pH 7.4 is very low in the absence of catalytic metals, such as iron and copper. Thus, the spontaneous oxidation of ascorbic acid can be used to test if low concentrations of catalytic iron or copper are present in PB or PBS solution.

Ascorbic acid (Sigma) was prepared freshly as a 0.1 M stock solution with redistilled water resulting in a colorless solution (pH 2). To perform the ascorbate test [Buettner GR, 1988], about 3.75 μ L of the ascorbate solution was mixed with 3 mL PB or PBS. A UV spectrophotometer was used to measure the absorbance at 265 nm. The initial absorbance at 265 nm is \approx 1.8; if adventitious metals are absent in the test solution, this absorbance should decrease by less 0.5% in 15-30 min.

Spin Traps

The spin trap DMPO, 5,5-dimethyl-pyrroline-1-oxide (Sigma) was first purified with activated charcoal/benzene [Kotake Y, 1994], and then prepared as a 1.0 M aqueous stock solution. During the experiment this DMPO stock solution was kept on ice. DMPO (50 mM) was used for the DHA experiments, 100 mM used for LDL experiment, and 100-150 mM used for cell experiments. The spin trap 5-diethoxyphosphoryl-5-methyl-1-pyrroline-N-oxide (DEPMPO), purchased from Oxis International Inc. (Chicago, IL), was diluted to the experimental concentration immediately before the spin trapping experiment. About 2 μ L DEPMPO solution was added to prepare 500 μ L EPR samples, yielding a final concentration of 16 mM DEPMPO.

Fe²⁺ and Cu²⁺ Solutions

Ferrous ammonium sulfate (Fe(NH₄)₂ (SO₄)₂ • 6H₂O) and copper sulfate (CuSO₄ • 5H₂O), purchased from Fisher, were used to prepare the 10 mM Fe²⁺ and Cu²⁺ stock solutions with redistilled water. To keep Fe²⁺ and Cu²⁺ stable, the pH of these stock solutions was adjusted at about 2.5 with 1N HCl.

Chelators

Diethylenetriaminepentaacetic acid (DTPA, Sigma) was dissolved in redistilled water by moderate heating to make 10 mM neutral stock solutions. When DTPA-Fe²⁺

solution was used, the ratio of DTPA:Fe²⁺ was 1.1:1.

Docosahexaenoic Acid (DHA)

Docosahexaenoic acid (DHA, Sigma) was prepared as a 1.25 to 5 mM aqueous stock solution immediately before EPR spin trapping experiments. For special purposes, the DHA stock solution was first exposed by air for 16-24 h autooxidation.

Photofrin

Photofrin stock solution (porfimer sodium, QLT, Phototherapeutics, Inc., Vancouver, BC, Canada) was dissolved in 5% dextrose (3 mg/mL, pH 7.4), sterile-filtered and stored at -20°C. For the Photofrin treatment, K-562 cells were incubated with Photofrin (6-9 µg/mL) for 45 min in PBS solution; MCF-7 cells were incubated with Photofrin (6 µg/mL) for 24 h in full medium.

Low-Density Lipoprotein (LDL)

Low-density lipoprotein was obtained from Dr. S. Hempel's Lab, University of Iowa. EDTA (1 mg/mL) was present throughout the isolation and dialysis to prevent LDL oxidation. A typical incubation for EPR experiments consisted of 2.2 mg/mL of LDL, 100 mM DMPO, and 100 µM Cu²⁺ in PB. To analyze spin adducts in the PB-LDL suspension, the incubation mixture (500 µL) was transferred into an EPR flat cell for EPR measurement. For analysis of spin adducts in the lipid portion of LDL, the incubation mixture (500 µL) was extracted by Folch extraction before EPR measurement.

Suspension Cells

Human erythroid leukemia cells (K-562 cells) were grown in RPMI 1640 medium (Grand Island Biochemical Co. Grand Island, NY) containing 10% fetal bovine serum (FBS, Sigma). Cell lipids were modified by supplementation of the medium with 32 µM

DHA for 48 h [Guffy MM, 1984; Burns CP, 1991; 1988]. Before the oxidation experiments, cells were washed three times with PBS and resuspended in 500 μ L PBS with 100 mM DMPO (5 min) at a density of 5×10^6 or 2×10^7 cells/mL. After oxidative stress, such as Photofrin treatment, light treatment, and addition of Fe^{2+} , PBS-suspended cells were either directly transferred into an EPR flat cell for measurement of radical formation, or subjected by the Folch extraction before EPR detecting lipid radicals in organic phase.

Adherent Cells

Human breast adenocarcinoma cells (MCF-7, parental wild type cells) and MCF-7 cells that overexpress the mitochondrial form of phospholipid hydroperoxide glutathione peroxidase (PhGPx) were cultured in minimal essential medium (MEM) containing 10% fetal bovine serum (FBS), 1% MEM non-essential amino acid, 30 nM sodium selenite, and 0.35 mg/mL G418. The overexpressing PhGPx cell lines were established by stable transfection of MCF-7 cells with the human mitochondrial form of PhGPx cDNA and pcDNA3.1(-) using LipofectAmine method (Life Technologies, Inc., Gaithersburg, MD). All the transfectants have been screened for PhGPx expression by western and northern analysis [Wang H, 1999].

After cells were grown in 100 mm dishes until 80% confluent, they were incubated with Photofrin for 24 h, washed 3 times with PBS, and illuminated with visible light in PBS. PBS then was replaced by full medium to reincubate cells for 6 h at 37°C in the dark. DMPO (150 mM) was added to cells, and 5 min later Fe^{2+} (100 μ M) was added to initiate radical reactions. The supernatant was transferred into an EPR flat cell at desired time points and was measured by EPR. Methanol (3 mL) was immediately added to the cell dish for scraping cells off, and then immediately transferred into extraction tube for Folch extraction. After phase separation, the lipid portion was dried by N_2

purging, and resuspended in a degassed E.A., then the lipid radicals in the organic phase were detected by EPR.

Methods

The Order of Addition

The order of addition of reaction reagents is an important factor that can affect the results. In our experiments, the target materials were usually mixed with PBS or PB before introducing any other reagents. The spin trap DMPO or DEPMPO was then added to the system and incubated for 2-5 min. The Fe²⁺ solution was always added to the oxidation system last.

EPR Measurement

The EPR samples (500 μ L) consisted of 1.25-5 mM DHA in PB; 2.2 mg/mL LDL in PB; or K-562 cells (5×10^6 or 2×10^7 cells/mL) suspended in PBS. Two or five min after the introduction of DMPO or DEPMPO into the sample, oxidative stress was initiated and the sample was immediately transferred into a flat cell for EPR measurement. For the EPR detection of lipid radicals in the organic phase, the solution was always purged with N₂ to remove oxygen that causes line-broadening. All EPR spectra were obtained with a Bruker ESP-300 spectrometer operating at 9.76 GHz and room temperature. The EPR spectrometer settings were: modulation frequency 100 kHz; modulation amplitude 1.0 G; microwave power 40 mW, and receiver gain 10^5 - 10^6 . To assist in the assignment of spin adducts, comparisons were made with published values tabulated in the Spin Trapping Database at <http://epr.niehs.nih.gov/stdb1.html>, as well as other tabulations [Li ASW, 1988; Buettner GR, 1987].

Ethyl Acetate Extraction

The DHA samples (500 μ L) were extracted with 3 mL ethyl acetate (saturated with ice cold water). Samples were kept at room temperature until phase separation (30 min–2 h). The upper ethyl acetate phase was transferred into a 10 mL glass tube and evaporated with N_2 or Ar. The dry residue was re-suspended in 500 μ L nitrogen-saturated E.A. for EPR measurement of lipid radicals.

Folch Extraction for LDL and K-562 Cells

LDL (2.2 mg/mL) or K-562 cells (5×10^6 cells/mL) in 500 μ L PB or PBS were extracted with ice cold methanol (3 mL): $CHCl_3$ (6 mL):0.9% saline (1.5 mL). Samples were kept at room temperature overnight to allow phase separation. The bottom phase ($CHCl_3$) was transferred into 15 mL glass tubes and purged with nitrogen. After complete evaporation, the lipid residue was re-suspended in 500 μ L nitrogen-saturated E.A. for EPR measurement of lipid radicals.

Folch Extraction for MCF-7 Cells

After Photofrin/light treatment, cells were subjected to ferrous iron, and the PBS was removed. The cells were harvested by scraping with 3 mL of ice cold methanol and then immediately transferred into extraction tubes where $CHCl_3$ (6 mL) and 0.9% NaCl (2 mL) were present. Allowing phase separation overnight, the $CHCl_3$ layer with the lipid portion of the cells was transferred into glass tubes and evaporated with N_2 . Degassed E.A. (500 μ L) was used to resuspend the lipid portion of the cells for EPR measurement.

Photofrin/Light Treatment

K-562 cells were incubated with Photofrin (6-9 μ g/mL) for 45 min in PBS solution. After Photofrin-treatment, K-562 cells were washed three times with PBS, and then exposed to the visible light (180 J/m^2s , 0-20 min) in PBS.

MCF-7 cells were incubated with Photofrin (6 $\mu\text{g}/\text{mL}$) for 24 h in full medium. After washing with PBS three times, the Photofrin-treated cells were resuspended in PBS and then exposed to light (5 $\text{J}/\text{m}^2\text{s}$, 5 min). After light treatment, MCF-7 cells were incubated with culture medium for 6 h.

Oxygen Monitor

A YSI Model 5300 Biological Oxygen Monitor (Yellow Springs Instruments, Yellow Springs, OH) was used to measure oxygen consumption during oxidation of DHA and cell membranes.

Anaerobic Suspension

The oxygen in the sample solution or other reagent solutions was removed by N_2 purging for 2-5 min to produce a near anaerobic suspension system. With the techniques used, oxygen level were 1%, 2.5 μM , or less in the anaerobic suspensions.

CHAPTER III

EPR STUDY OF DHA PEROXIDATION

Polyunsaturated lipids are cellular macromolecules that can be easily damaged during oxidative stress. They can undergo peroxidation, producing free radicals that can be detrimental to cells. To understand the free radical mechanism behind cellular membrane peroxidation, we used the EPR spin trapping method to detect lipid-derived radicals. There are two kinds of lipid-derived radicals (L_d^\bullet) formed during lipid peroxidation (Scheme 1). One type is the carbon-centered radicals, which includes lipid alkyl (L^\bullet), β -scission alkyl (R^\bullet), and epoxyallylic (OL^\bullet) radicals. Another is the oxygen-centered radicals including alkoxy (LO^\bullet/RO^\bullet), peroxy (LOO^\bullet/ROO^\bullet), and epoxyperoxy ($OLOO^\bullet$). As shown in Schemes 1-3, if O_2 and Fe^{2+} are present, the lipid peroxidation process will cycle, resulting in the continuation of lipid-derived radical production. Thus, in EPR spin trapping studies of lipid peroxidation, the lipid-derived radicals will undergo various termination reactions (reactions 5-9, and reaction 19) that compete with the spin trapping reaction (reaction 18). The lipid-derived radicals will also react with the DMPO spin adducts that have been formed (reaction 20). From a kinetic point of view, reaction 20 should be a significant route to the destruction of spin adducts formed during lipid peroxidation [Kocherginsky N, 1995]. We propose that, during lipid peroxidation, the successful EPR detection of lipid-derived radicals depends on careful experimental design taking into account the kinetics of both the formation and termination processes of spin adducts.

In order to succeed in the EPR observation of lipid-derived radicals in cellular

membrane peroxidation, docosahexaenoic acid (DHA) was used as a simplified model for EPR studies of the lipid peroxidation process. Two nitron spin traps, 5,5-dimethyl-pyrroline-1-oxide (DMPO) and 5-diethoxyphosphoryl-5-methyl-1-pyrroline-N-oxide (DEPMPO) were used in the effort to detect the many possible lipid-derived radicals formed during Fe^{2+} -mediated DHA oxidation.

DMPO in a DHA-Suspension Study

Figure 1A shows a typical EPR spectrum that can be observed from the Fe^{2+} -mediated oxidation of DHA in aerobic suspension. There are four different species in Figure 1A, labeled 1, 2, 3, and 4. By comparing our observations with published values from the spin trapping database at <http://epr.niehs.nih.gov/stdb1.html> and other sources [Li ASW, 1988; Buettner GR, 1987], these radical adducts were assigned as two carbon-centered radicals ($a^{\text{N}}_1 \approx 15.8 \text{ G}$, $a^{\text{H}}_1 \approx 22.6 \text{ G}$; $a^{\text{N}}_2 \approx 15.2 \text{ G}$, $a^{\text{H}}_2 \approx 18.9 \text{ G}$) and two oxygen-centered radicals ($a^{\text{N}}_3 \approx a^{\text{H}}_3 \approx 14.8 \text{ G}$; $a^{\text{N}}_4 \approx 14.6 \text{ G}$, $a^{\text{H}}_4 \approx 10.2 \text{ G}$ and 1.3 G). The computer simulated spectrum of Figure 1A is shown in Figure 1B, and the computer simulated EPR spectrum of each species is shown in Figures 1C-1F.

However, the observation of the spectrum in Figure 1A was time-limited. Generally, it lasts only about 1-2 min in aerobic DHA suspension due to the very short lifetimes of most DMPO radical adducts. Species 1, the carbon-centered radical adduct ($a^{\text{N}}_1 \approx 15.8 \text{ G}$; $a^{\text{H}}_1 \approx 22.6 \text{ G}$) has the longest lifetime. Species 3, the oxygen-centered radical adduct, *e.g.* alkoxyl-type radical adduct ($a^{\text{N}}_3 \approx a^{\text{H}}_3 \approx 14.8 \text{ G}$) has an intermediate lifetime. Species 2 and 4, the carbon-centered radical adduct ($a^{\text{N}}_2 \approx 15.2 \text{ G}$, $a^{\text{H}}_2 \approx 18.9 \text{ G}$) and the oxygen-centered radical adduct, *e.g.* peroxy-type radical adduct ($a^{\text{N}}_4 \approx 14.6 \text{ G}$, $a^{\text{H}}_4 \approx 10.2 \text{ G}$ and 1.3 G) have the shortest lifetimes. The lifetimes of these spin adducts can be varied with the different oxidation conditions in the suspension including the

oxygen profile and the reactant concentration. For example, the level of oxygen in a DHA

Figure 1. EPR spectra of DMPO/L_d• formed from the Fe²⁺-mediated oxidation of DHA in aerobic suspension. The control experiments in which DHA was absent produced no observable spin adducts. This spectrum is representative of at least five different experiments at this DHA concentration. In similar experiments the DHA concentration was varied from 0.1 mM to 10 mM. The principal differences observed were only in the EPR signal intensity.

- A: The sample contains 5 mM DHA, 50 mM DMPO, 110 μM DTPA, and 100 μM Fe²⁺. The EPR spectrum was collected beginning 1 min after Fe²⁺ addition; and was from 12 signal-averaged scans collected over a total of 2 min;
- B: Computer simulated EPR spectrum. The composite simulation for the species 1 to species 4 was used ratio of 0.5:0.5:0.7:1.0, and Linewidth ≈ 1.0 G, Lorentzian/Gaussian ≈ 1.0;
- C: Computer simulated carbon-centered radical adduct (species 1 in A):
 $a_1^N \approx 15.8$ G, $a_1^H \approx 22.6$ G;
- D: Computer simulated carbon-centered radical adduct (species 2 in A):
 $a_2^N \approx 15.2$ G, $a_2^H \approx 18.9$ G;
- E: Computer simulated alkoxy-type radical adduct (species 3 in A):
 $a_3^N \approx a_3^H \approx 14.8$ G;
- F: Computer simulated peroxy-type radical adduct (species 4 in A):
 $a_4^N \approx 14.6$ G, $a_4^{H\beta} \approx 10.2$ G; $a_4^{H\gamma} \approx 1.3$ G.

A: DHA oxidation in aerobic suspension, 1 min after Fe^{2+}



B: Computer simulation (species 1:2:3:4 \approx 0.5:0.5:0.7:1)



C: Species 1 (carbon-centered radical adduct)



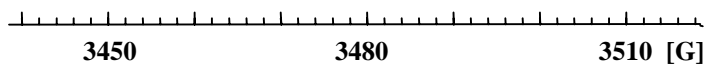
D: Species 2 (carbon-centered radical adduct)



E: Species 3 (alkoxyl-type radical adduct)



F: Species 4 (peroxyl-type radical adduct)



suspension can greatly alter the lifetimes of radical adducts, especially the lifetimes of the oxygen-centered radical adducts.

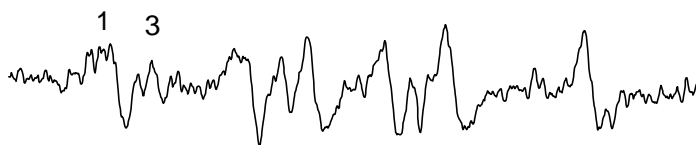
DHA Oxidation in Anaerobic Suspension

Figure 2 shows the results of Fe^{2+} -mediated DHA anaerobic oxidation by collecting EPR spectra at different time points (1, 5, and 20 min). Because little or no oxygen is available in this system, species 4, *e.g.* the adduct of peroxy-type radical ($a^{\text{N}}_4 \approx 14.6$ G, $a^{\text{H}}_4 \approx 10.2$ G and 1.3 G) could not be observed. However, species 3, another oxygen-centered radical adduct ($a^{\text{N}}_3 \approx a^{\text{H}}_3 \approx 14.8$ G), was a detectable species within the first 2-3 min after addition of ferrous iron (Figure 2A). We assigned species 3 as either the DMPO adduct of lipid alkoxyl radical (LO^\bullet) or $\text{DMPO}/\text{OH}^\bullet$, which are the only two oxygen-centered radical adducts that can form in this DHA anaerobic oxidation. Lipid alkoxyl radical (LO^\bullet) could be formed by the reaction of ferrous iron and lipid hydroperoxides (reaction 4), which exist in DHA suspensions formed through PUFA autooxidation. $\text{DMPO}/\text{OH}^\bullet$ can be formed by a non radical mechanism [Hanna PM, 1992].

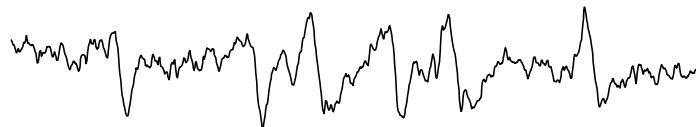
The dominant species detected in DHA anaerobic oxidation was species 1, the carbon-centered radical adduct ($a^{\text{N}}_1 \approx 15.8$ G, $a^{\text{H}}_1 \approx 22.6$ G). It is very stable so that it can be observed for hours. See Figure 2B and C. The computer-simulated spectrum of this species is shown as Figure 2D. We assigned species 1 as the adduct of an alkyl radical (R^\bullet) derived from the β -scission of lipid alkoxyl radical (LO^\bullet) (reactions 4, 16, and 17), because this alkyl radical (R^\bullet) is the only carbon-centered radical being produced during DHA anaerobic oxidation.

Like species 4, species 2 (carbon-centered radical adduct: $a_2^{\text{N}} \approx 15.2$ G, $a_2^{\text{H}} \approx 18.9$ G) was also not detected in this system. This result indicates that both species share a similar property in that their observation is dependent upon the presence of oxygen.

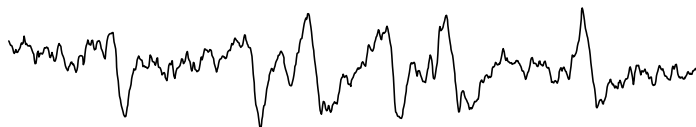
A: DHA oxidation in anaerobic suspension, 1 min after Fe^{2+}



B: 5 min after A



C: 20 min-1 h after A



D: Computer simulation of C

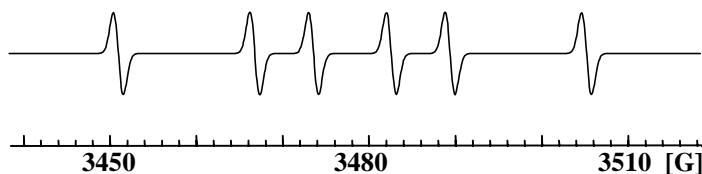


Figure 2. EPR spectra of $\text{DMPO}/\text{L}_d^\bullet$ formed from the Fe^{2+} -mediated DHA oxidation in anaerobic suspension. The sample contains 1.25 mM DHA, 50 mM DMPO, 55 μM DTPA, and 50 μM Fe^{2+} . All spectra are from 12 signal-averaged scans collected over a total of 2 min and are representative of at least five different experiments.

- A: The EPR spectrum was collected beginning 1 min after Fe^{2+} addition. There are two different spin adducts, species 1 and 3: $a_1^{\text{N}} \approx 15.8$ G, $a_1^{\text{H}} \approx 22.6$ G, $a_3^{\text{N}} \approx a_3^{\text{H}} \approx 14.8$ G;
- B: The EPR spectra were collected beginning 5 min after Fe^{2+} addition. Only species 1 can be clearly recognized;
- C: The EPR spectra were collected beginning 20 min after Fe^{2+} addition. Again, only species 1 can be clearly recognized;
- D: Computer simulated EPR spectrum of B or C using: $a_1^{\text{N}} \approx 15.8$ G, $a_1^{\text{H}} \approx 22.6$ G, Linewidth ≈ 1.0 G, and Lorentzian/Gaussian ≈ 1.0 .

Figure 3 shows a time profile of the DMPO lipid-derived radical adducts detected by EPR spin trapping in the Fe^{2+} -mediated DHA oxidation in anaerobic suspension. Note, only the radical profile with time (> 40 s) after Fe^{2+} addition is shown in Figure 3. Any radical formation and decay at times less than about 40 s will not be able to be determined in these experiments because the minimum time required for transferring the EPR sample and tuning the EPR is about 40 s.

DHA Oxidation in an Open Suspension

In an open system, the DHA suspension is always exposed to air, and thereby being reoxygenated. We assume that $[\text{O}_2]_{\text{ss}} \approx 250 \mu\text{M}$ in this suspension during an EPR experiment. We anticipated that when an open DHA suspension is subjected by Fe^{2+} treatment, the total production of DMPO adducts from lipid-derived radicals will be much greater than that in an anaerobic suspension system. A high steady-state $[\text{O}_2]$ in a DHA suspension leads to more radical propagation processes, thereby producing more lipid-derived radical adducts. By comparing Figures 3 and 4, the yield of most radical adducts in the open suspension was greater than in an anaerobic suspension, except for species 1, i.e. the carbon-centered radical adduct ($a^{\text{N}}_1 \approx 15.8$ G, $a^{\text{H}}_1 \approx 22.6$ G). This smaller yield of species 1 results from the competition of the reactions of the carbon-centered radical with the spin trap and oxygen [Buettner GR, 1995].

Figure 5 shows a time-dependent EPR spectrum observed from Fe^{2+} -mediated DHA oxidation in an open suspension. Species 4 (peroxyl-type radical adduct: $a^{\text{N}}_4 \approx 14.6$ G, $a^{\text{H}}_4 \approx 10.2$ G and 1.3 G) could only be observed first 5 min after the addition of ferrous iron (Figure 4A, B). The observation of species 3 (alkoxyl-type radical adduct $a^{\text{N}}_3 \approx a^{\text{H}}_3 \approx 14.8$ G) lasted as long as the observation of species 1, the carbon-centered radical adduct ($a^{\text{N}}_1 \approx 15.8$ G, $a^{\text{H}}_1 \approx 22.6$ G). See Figure 5D.

In an anaerobic system, we are able to assign species 1 as the DMPO adduct of a

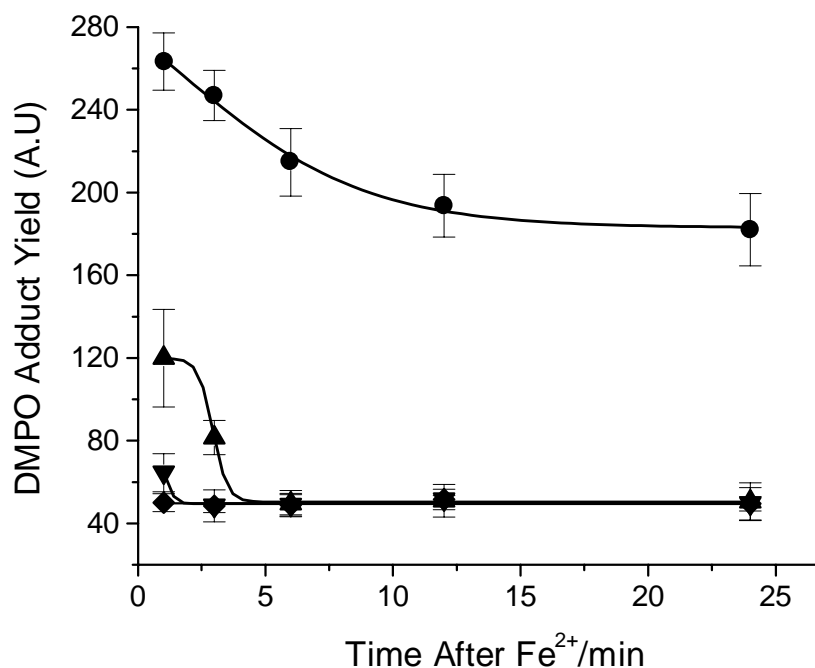


Figure 3. The profile of DMPO/ L_d^{\bullet} detected by EPR in Fe^{2+} -mediated DHA oxidation in an anaerobic PB suspension. The sample contains 1.25 mM DHA, 50 mM DMPO, 60 μ M DTPA, and 50 μ M Fe^{2+} . All incubations were purged with N_2 to make anaerobic conditions. In the Figure, ● represents carbon-centered radical adduct (species 1 in Figure 1A); ▼ represents carbon-centered radical adduct (species 2 in Figure 1A); ▲ represents alkoxy-type radical adduct (species 3 in Figure 1A); and ◆ represents peroxyl-type radical adduct (species 4 in Figure 1A). The background noise-level of the EPR spectrum signal is about 50 A.U.; thus, a yield around 50 A.U. was considered to be no significant radical production. The DMPO adduct yield is represented as the EPR signal height from 12 signal-averaged scans collected over a total of 2 min, $n = 3$. Error bars represent standard deviation.

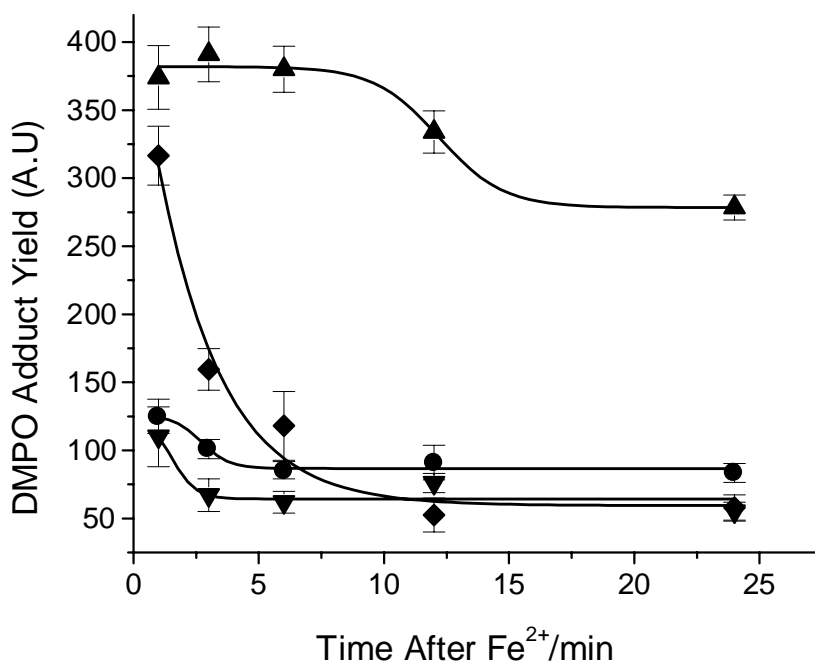


Figure 4. The profile of DMPO/ L_d^{\bullet} detected by EPR in Fe^{2+} -mediated DHA oxidation in open suspension. The sample contains 1.25 mM DHA, 50 mM DMPO, 60 μ M DTPA, and 50 μ M Fe^{2+} . In the open system, we assumed that $[O_2]_{ss} \approx 250 \mu$ M. In the Figure, ● represents carbon-centered radical adduct (species 1 in Figure 1A); ▼ represents carbon-centered radical adduct (species 2 in Figure 1A); ▲ represents alkoxy-type radical adduct (species 3 in Figure 1A); and ◆ represents peroxy-type radical adduct (species 4 in Figure 1A). The background noise-level of the EPR spectrum signal is about 50 A.U.; thus, a yield around 50 A.U. was considered to be no significant radical production. The DMPO adduct yield is represented as the EPR signal height from 12 signal-averaged scans collected over a total of 2 min, $n = 3$. Error bars represent standard deviation.

Figure 5. EPR spectra of DMPO/L_d• formed during Fe²⁺-mediated DHA oxidation. The spectrum changes with time indicating an evolving balance between adduct formation and adduct decay. In the open system we assumed the [O₂]_{ss} is about 250 μM. All spectra are from 12 signal-averaged scans collected over a total of 2 min and are representative of at least five different experiments.

- A: EPR spectrum from 1.25 mM DHA incubated with 50 mM DMPO, 55 μM DTPA, and 50 μM Fe²⁺. This EPR spectrum was collected beginning 1 min after Fe²⁺ addition. There are four different spin adducts: $a_1^N \approx 15.8$ G, $a_1^H \approx 22.6$ G; $a_2^N \approx 15.2$ G, $a_2^H \approx 18.9$ G, $a_3^N \approx a_3^H \approx 14.8$ G; $a_4^N \approx 14.6$ G, $a_4^{H\beta} \approx 10.2$ G; $a_4^{H\gamma} \approx 1.3$ G;
- B: EPR spectrum from sample A, but spectrum collection was initiated 5 min after Fe²⁺ addition. This spectrum shows a loss of DMPO adducts compared with A;
- C & D: EPR spectrum from sample A, but collection was initiated 20 min and 3 h after Fe²⁺ addition. There are two radical adducts can be detected in those time points. Their hyperfine spin splittings are: $a_1^N \approx 15.8$ G, $a_1^H \approx 22.6$ G; and $a_3^N \approx a_3^H \approx 14.8$ G;
- E: Computer simulated EPR spectrum of D. The ratio of carbon-centered radical adduct and alkoxy-type radical adduct is: 1:1 (Linewidth ≈ 1.0 G, and Lorentzian/Gaussian ≈ 1.0).

A: 1 min after Fe^{2+} :



B: 5 min after Fe^{2+} :



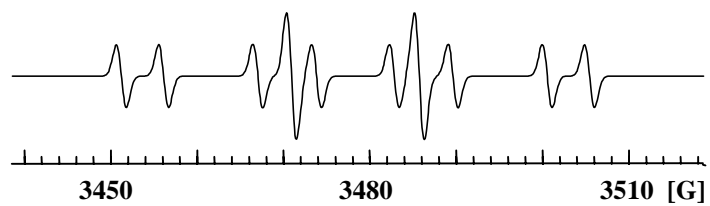
C: 20 min after Fe^{2+} :



D: 3 h after Fe^{2+} :



E: Computer simulation of D: species 1: species 3 \approx 1:1



β -scission alkyl radical (R^\bullet), and assign species 3 either as the DMPO adduct of lipid alkoxy radical (LO^\bullet) or DMPO/ $^\bullet OH$. However, during DHA aerobic oxidation, there are more radicals that can be formed and that have hyperfine splitting constants similar to those of species 1 and 3. For example, lipid alkyl radical (L^\bullet), the initial carbon-centered radical formed from the lipid chain after loss of H atom, should have hyperfine splitting constants similar to species 1. However, we exclude DMPO/ L^\bullet in our DHA aerobic oxidation, because L^\bullet will react with oxygen (reaction 2) with a diffusion rate [Hasegawa K, 1978], much faster than its reaction with spin trap.

Like in an anaerobic system, species 2 (another carbon-centered radical adduct: $a^N_2 \approx 15.2$ G, $a^H_2 \approx 18.9$ G) appeared and disappeared along with species 4 (peroxy-type radical adduct: $a^N_4 \approx 14.6$ G, $a^H_4 \approx 10.2$ G and 1.3 G) in this system. Based on its hyperfine splitting constants and its oxygen-dependent property, we propose that species 2 is derived from the β -scission of lipid alkoxy radical, either the adduct of OL^\bullet or the adduct of OR^\bullet . Again, it is impossible to be specific as to which of them was trapped based on the current data. Thus, species 2 may be any one of OL^\bullet and OR^\bullet , or their combination.

Based on published data, species 3 may be any one of the DMPO adducts of LO^\bullet , RO^\bullet , and HO^\bullet , or it may be any combination of these adducts.

Although species 4 is proposed [Dikalov SI, 1999] to be an alkoxy radical adduct in some chemical models, we have tentatively assigned species 4 in our DHA system as a peroxy-type radical adduct. This species may include DMPO adducts of LOO^\bullet , $OLOO^\bullet$, and $^\bullet OOH$ not only due to their hyperfine splitting constants but also because of their much longer lifetime compared to the chemical models used in Dikalov's paper.

The results from the open system indicate that when a high steady-state concentration of oxygen is available, the detection of lipid peroxy-type radicals still has

serious problems due to their short lifetimes. It is also difficult to specify exactly which radical adduct is being observed because similar adducts have similar hyperfine splitting constants. Failure to have this oxygen-centered radical analysis and failure to determine the real time profile of each detectable species in the lipid peroxidation severely inhibits our ability to gain knowledge about radical events in lipid peroxidation.

DHA Oxidation in Closed (Air-Saturated) Suspension

Figure 6 shows the time profile of the four lipid radical adducts detected by EPR from the Fe^{2+} -mediated DHA oxidation in an air-saturated suspension system. The total adduct production in the closed (air-saturated) DHA system was generally between that of the open-system and the anaerobic system (Figure 7). Again, however, species 1 (carbon-centered radical: $a^{\text{N}}_1 \approx 15.8 \text{ G}$, $a^{\text{H}}_1 \approx 22.6 \text{ G}$), the thatched portion in Figure 7 is less at a higher oxygen concentration. It is interesting that in a long-term process (Figure 7C), total production of adducts in a closed system is less than that in an anaerobic system (first two bars in Figure 7C, 317 vs. 333). The system with more oxygen should have more propagating ability, leading to more radical production. The phenomenon that high $[\text{O}_2]_{\text{ss}}$ leads to less radical production is incompatible to the basic concept of lipid peroxidation.

The result that high $[\text{O}_2]_{\text{ss}}$ leads to less detectable spin adduct draws our attention to the significance of the destruction of spin adducts (reaction 20). We propose that the termination reaction of spin adducts plays a key role in the failure of EPR detection of lipid radicals in lipid peroxidation. We believe that the observation that high $[\text{O}_2]_{\text{ss}}$ results in a less radical detection does not mean less actual radical production. Rather, more radical reactions will result in more radicals being trapped, but also more destruction of spin adducts. At some stage, adduct destruction processes (reaction 20) will kinetically play a dominant role in destroying the spin adducts that have been

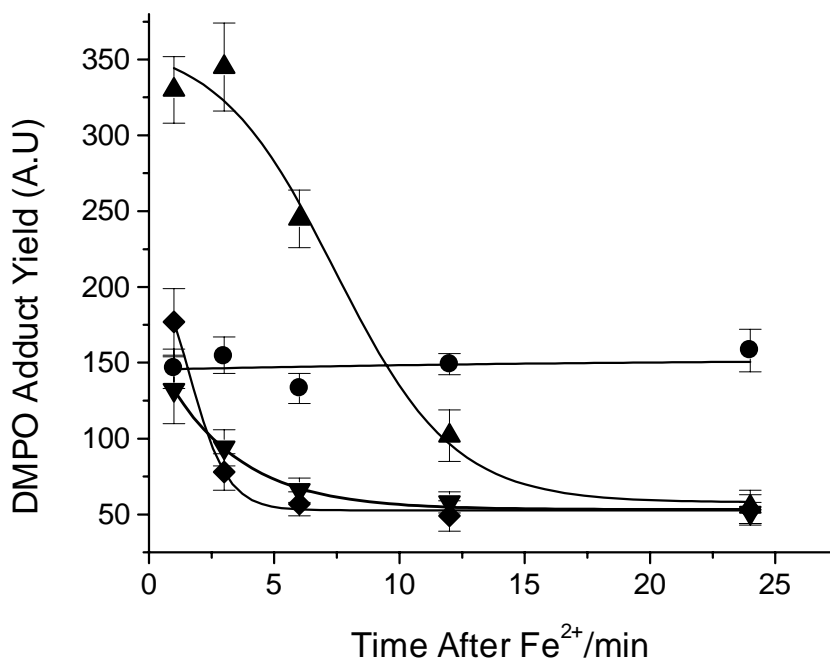
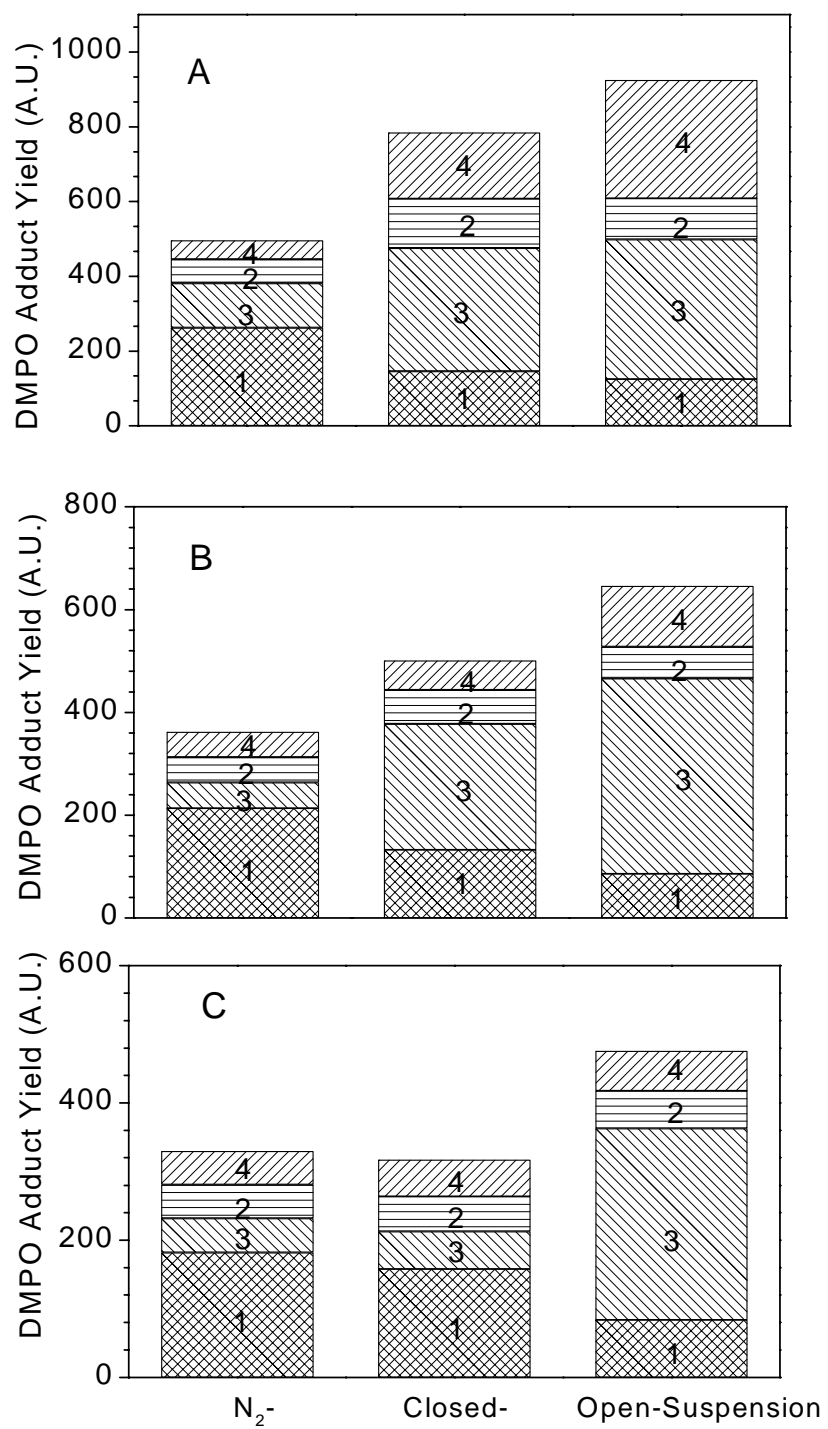


Figure 6. The profile of DMPO/L_d detected by EPR in Fe²⁺-mediated DHA oxidation in closed, air-saturated suspension. The sample contains 250 μM O₂, 1.25 mM DHA, 50 mM DMPO, 60 μM DTPA, and 50 μM Fe²⁺. In the Figure, ● represents carbon-centered radical adduct (species 1 in Figure 1A); ▼ represents carbon-centered radical adduct (species 2 in Figure 1A); ▲ represents alkoxy-type radical adduct (species 3 in Figure 1A); and ◆ represents peroxyl-type radical adduct (species 4 in Figure 1A). The background noise-level of the EPR spectrum signal is about 50 A.U.; thus, a yield around 50 A.U. was considered to be no significant radical production. The DMPO adduct yield is represented as the EPR signal height from 12 signal-averaged scans collected over a total of 2 min, n = 3. Error bars represent standard deviation.

Figure 7. The comparison of all adduct yields formed in the three different oxygen profiles, e.g. N₂-, air-saturated and open systems. In the bars, × represents species 1; \\\ represents species 3; ≡ represents species 2; /// represents species 4. The yield of 50 A.U. represents the EPR background signal, n = 3. The standard deviation is similar to those observed in Figure 6.

- A: EPR spectrum gathered beginning 1 min after addition of ferrous iron;
- B: EPR detection gathered 5 min after addition of ferrous iron;
- C: EPR detection gathered 25 min after addition of ferrous iron.



formed.

We also found that the total DMPO adduct yield in each oxygen profile decreased with the time. For example, the total adduct yield in closed-system (middle bars in Figure 7A-C) is reduced from 785 A.U. (1 min oxidation) to 317 A.U. (25 min oxidation). This result again suggests that termination reaction 20 plays an important role in destroying spin adducts.

In order to correlate the oxygen radical adducts and the oxygen profile in suspension solution during lipid peroxidation, the oxygen monitor was used to determine the depletion of oxygen in a closed, air-saturated system. The initial $[O_2]$ of this system is considered to be about 250 μM .

Figure 8 shows an oxygen monitor experiment of Fe^{2+} -mediated DHA oxidation. About 25% of the oxygen in the suspension is consumed within the first min after addition of ferrous iron. Following this initial fast depletion of oxygen, oxygen was then consumed at very stable rate. We estimated that about 60 μM $[O_2]$ was consumed during the initiation steps (1 min) to form iron-oxygen complexes and to form oxygen-centered radicals; about 190 μM $[O_2]$ remained to drive the radical propagation reactions at nearly constant rates (1.7 $\mu\text{M}/\text{min}$). Based on this observation, we think that the radical profile within the first 1 min is very important for understanding the roles of the various radicals in lipid peroxidation. Furthermore, due to the detrimental role of peroxy radical in lipid peroxidation and its short life, we must improve its detection.

The ability to detect species 4 has severe limitations in a closed system. Figure 9 shows the time-dependent appearance and disappearance of the lipid-derived radical adducts in Fe^{2+} -mediated DHA oxidation in a closed (air-saturated) system; compared to the open-system in Figure 5. Species 2 (adduct of OL^\bullet , OR^\bullet , or their combination), and

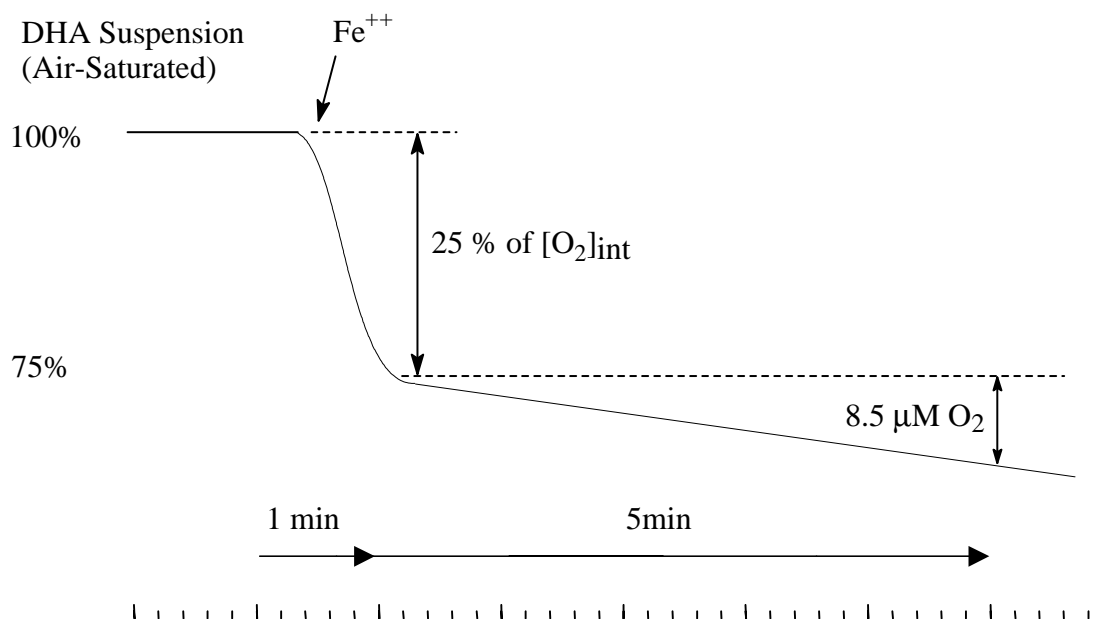


Figure 8. O_2 depletion experiment in Fe^{2+} -mediated DHA oxidation. The system contains 1.25 mM DHA, 250 $\mu\text{M } [\text{O}_2]_{\text{int}}$, and 50 $\mu\text{M } \text{Fe}^{2+}$. 25% of oxygen (60 μM) is depleted during first 1 min. Then the oxygen is consumed at a very stable rate, 1.7 $\mu\text{M}/\text{min}$.

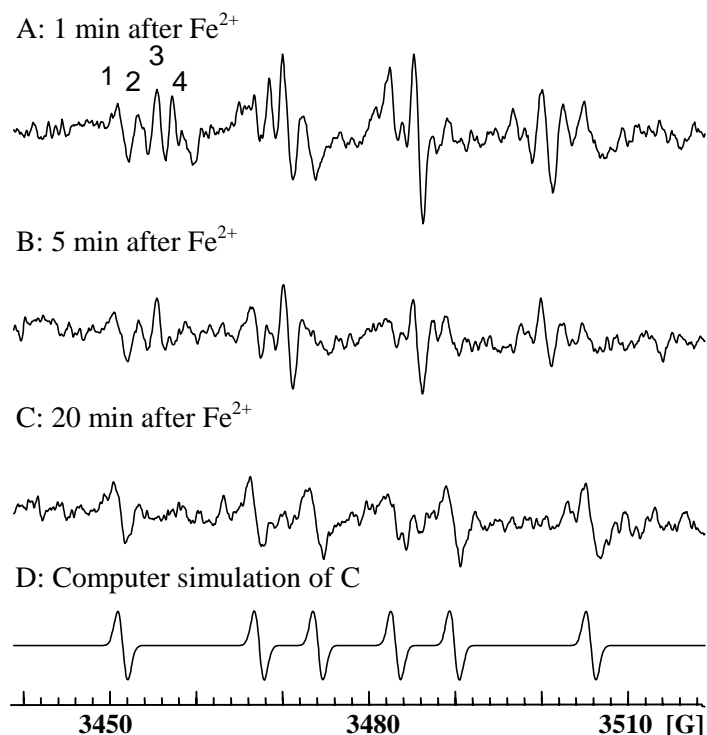


Figure 9. EPR spectra of DMPO/ L_d^\bullet formed from Fe^{2+} -mediated DHA oxidation in a closed (air-saturated) suspension. Spectra change with time indicating an evolving balance between adduct formation and adduct decay. All spectra are from 12 signal-averaged scans collected over a total of 2 min and are representative of at least five different experiments.

- A: EPR spectrum from 1.25 mM DHA incubated with 250 μ M O_2 , 50 mM DMPO, 60 μ M DTPA, and 50 μ M Fe^{2+} . This EPR spectrum was collected beginning 1 min after Fe^{2+} addition. There are four different spin adducts: $a_1^N \approx 15.8$ G, $a_1^H \approx 22.6$ G; $a_2^N \approx 15.2$ G, $a_2^H \approx 18.9$ G, $a_3^N \approx a_3^H \approx 14.8$ G; $a_4^N \approx 14.6$ G, $a_4^{H\beta} \approx 10.2$ G; $a_4^{H\gamma} \approx 1.3$ G;
- B: EPR spectrum from sample A, but spectrum collection was initiated 5 min after Fe^{2+} addition. This spectrum shows a loss of DMPO adducts compared with A;
- C: EPR spectrum from sample A, but collection was initiated 20 min after Fe^{2+} addition. Only the one radical adduct ($a_1^N \approx 15.8$ G, $a_1^H \approx 22.6$ G) can be detected in this time;
- D: Computer simulation of EPR spectrum of C.

species 4 (adduct of LOO^\bullet , OLOO^\bullet , ROO^\bullet , $\text{}^\bullet\text{OOH}$, or their combination) have the shortest lifetimes (< 2 min). Species 3, DMPO adducts of LO^\bullet , RO^\bullet , $\text{}^\bullet\text{OH}$, or their combination, have intermediate lifetimes, about 2-5 min. Species 1, e.g. β -scission alkyl radical, was observed with the longest lifetime (> 4 h) in closed, DHA suspension.

Summary of DMPO in DHA Suspension Study

These four species can only be observed within a very short time period (2-3 min) in the oxidation of a suspension of DHA. Thus, the EPR analysis of these radicals has severe time limitations. In addition, it is a problem to specify exactly which radical adduct is present due to the fact that many radical adducts have similar hyperfine splitting constants. In the DHA suspension, we have only been able to clearly identify species 1 as R^\bullet , *i.e.* a fragment alkyl radical. However, the exact identification of the other species is not yet possible. For example, species 2 may be DMPO adducts of OL^\bullet , and/or OR^\bullet ; species 3 may be DMPO adducts of LO^\bullet and/or $\text{}^\bullet\text{OH}$; species 4 may be DMPO adducts of LOO^\bullet , OLOO^\bullet , ROO^\bullet , and/or $\text{}^\bullet\text{OOH}$.

Because of the big mismatch between the oxygen profile in DHA suspension (Figure 8) and the spin adducts of the lipid-derived oxygen-centered radicals (Figure 9), there is great uncertainty in what we can learn from these experiments. In other words, the observed spin adduct profile may not reflect actual radical flux at a given time. Not being able to determine the first 40 s of the radical profile is the another a big deficiency in the EPR study of the oxidation of DHA in suspension.

We hypothesize that the interruption of the termination reaction (reaction 20) will play a key role in the successful study of the reactions of oxygen-centered lipid radicals. We propose that coupling an extraction process with EPR spin trapping would interrupt reaction 20 and increase the usefulness of EPR studies of lipid peroxidation.

DMPO Study and E.A. Extraction

We have developed an extraction method (Scheme 3) to separate the oxidizable substrate (lipids) from the mediator of oxidation (iron). Due to the highly hydrophilic nature of DMPO, we anticipated that the unreacted DMPO would remain in the aqueous phase, being separated from the organic phase after extraction. Separation will interrupt the lipid peroxidation processes, thereby stabilizing the DMPO/L_d[•] spin adducts by minimizing reaction 20 and by diluting reactants. We anticipate that many of the disadvantages of the EPR study of our DHA suspension would be overcome by this extraction protocol. For example, the radical profile can be determined within the initiation period (< 40 s) of lipid peroxidation, which is not possible in the DHA suspension study. We also expect that our extraction will allow us to distinguish radical adducts *via* their hydrophilic or hydrophobic nature, in addition to their hyperfine splitting constants.

Theoretically, the extraction separates radical adducts according to their affinities for either water or lipids. The adducts with long lipid chains will partition to the organic phase, and adducts with fragmental-short chains will partition into the aqueous phase, see Table 2. The goal of our extraction protocol is to separate radical adducts in a way that the longer chain lipid radical adducts (DMPO/OLOO[•], LOO[•], OL[•], L[•], LO[•]) will be in the E.A. phase, while non-lipid chain radical adducts (DMPO/ROO[•], [•]OOH, RO[•], R[•] HO[•]) will be in the aqueous phase after extraction. For example, adducts of OLOO[•]/LOO[•] and ROO[•]/HOO[•] have similar hyperfine splittings, but after extraction the former will be in the E.A. phase, while the latter will be in the water phase. Thus, we will be able to monitor the radical profile during lipid peroxidation, which will provide information necessary to understand the mechanism of lipid peroxidation.

Table 2. Extraction improves the identification of DMPO spin adducts

Species	Spin Adduct	Spin Adduct Location After Extraction
Species 1 ($a^N \approx 15.8$ G, $a^H \approx 22.6$ G)	DMPO/R \cdot	Aqueous Phase
	DMPO/L \cdot	E.A. Phase
Species 2 ($a^N \approx 15.2$ G, $a^H \approx 18.9$ G)	DMPO/OR \cdot	Aqueous Phase
	DMPO/OL \cdot	E.A. Phase
Species 3 ($a^N \approx a^H \approx 14.8$ G)	DMPO/OH \cdot	Aqueous/E.A.*
	DMPO/RO \cdot	Aqueous Phase
	DMPO/LO \cdot	E.A. Phase
Species 4 ($a^N \approx 14.6$ G, $a^H \approx 10.2, 1.3$ G)	DMPO/OOH \cdot	Aqueous/E.A.*
	DMPO/ROO \cdot	Aqueous Phase
	DMPO/LOO \cdot	E.A. Phase
	DMPO/OLOO \cdot	E.A. Phase

Note: L represents the long chain lipid radicals. R represents fragment, short chain radicals. * represents species which can be distributed between both E.A. phase and aqueous phase, but will be removed from the organic phase via N₂-purging and E.A. resuspension.

Location of DMPO and the DMPO Adducts After Extraction

We are interested in detecting the radical profile in real time. To do so, it is very important that the unreacted DMPO remains in the aqueous phase after extraction, because any DMPO in the organic phase would react with the radicals still being produced during the extraction, thereby changing the observed lipid radical profile. To verify the location of DMPO after E.A. extraction, we extracted a 100 μM aqueous solution of DMPO (Figure 10). UV spectra [Buettner GR, 1990] were used to determine the distribution of DMPO after extraction. The aqueous phase after the extraction was carefully purged with nitrogen to remove ethyl acetate, Figure 10 C-E. The spectrum of DMPO in the aqueous phase after N_2 -purging (30 min) shows that ethyl acetate has been completely removed. Figure 10E is nearly identical to the 100 μM aqueous solution of DMPO before extraction, Figure 10F. These data indicate that DMPO after E.A. extraction predominantly locates in the aqueous phase. Thus, the E.A. extraction can be used to separate the mediator of oxidation (chelated iron) and unreacted DMPO from lipid chain radicals, thereby minimizing the occurrence of background lipid oxidation and stopping the lipid peroxidation cycle. Figure 11 shows similar results of DMPO location after the extraction process using CHCl_3 as the organic solvent.

To confirm that the short chain radical adducts would remain in the aqueous phase we designed an experiment using DMSO as the radical source. This DMSO oxidation system contained 50 mM DMPO, 100 mM DMSO, 100 μM H_2O_2 , and 50 μM Fe^{2+} . Oxidation of DMSO is reported [Hanna PM, 1992; Makino K, 1990; Buettner GR, 1995] to produce $\text{DMPO}/\dot{\text{C}}\text{H}_3$, $\text{DMPO}/\dot{\text{O}}\text{C}\text{H}_3$, and $\text{DMPO}/\dot{\text{O}}\text{O}\text{C}\text{H}_3$ adducts. Figure 12 shows the distributions of these DMPO adducts after E.A. extraction. No EPR signal was detected in the E.A. phase, and all radical adducts from DMSO oxidation remained in the aqueous phase after extraction. These data are consistent with our hypothesis that all

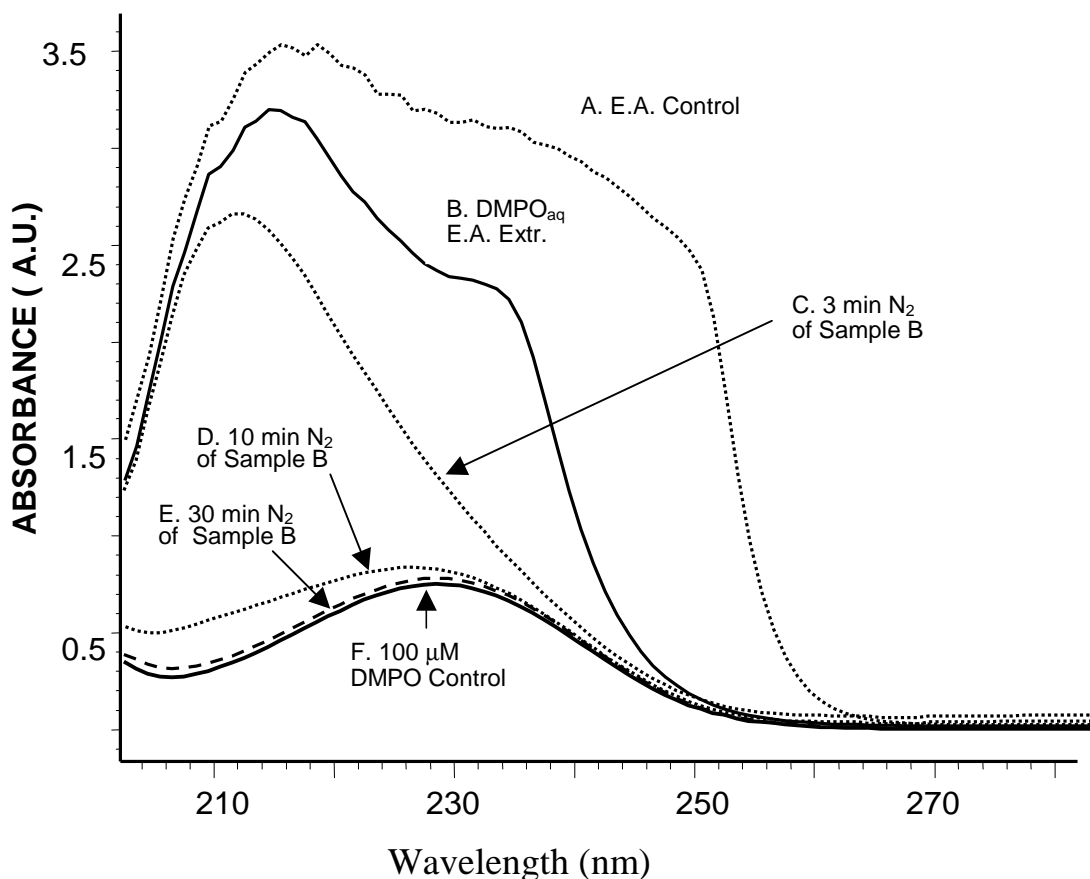


Figure 10. DMPO remains in the aqueous phase after E.A. extraction. (UV spectra of DMPO $\epsilon_{225\text{nm}} \approx 7800 \text{ M}^{-1} \cdot \text{cm}^{-1}$ [Buettner GR, 1990]).

- A: E.A. 100 %. Note, absorbance readings ≥ 2 are above the limits for reliability of the instrument;
- B: The UV spectra of 100 μM aqueous solution of DMPO after E.A. extraction ($\text{H}_2\text{O}/\text{E.A.} = 1/2$ (v/v));
- C: Sample B purged with N_2 gas for 3 min. The difference in the spectrum B and C demonstrates that the E.A. that partitioned into the buffer is being purged by N_2 ;
- D: Sample B after purging with N_2 gas for 10 min;
- E: Sample B after purging with N_2 gas for 30 min; virtually all ethyl acetate has been removed. The absorbance at 225 nm is comparable with the DMPO solution before extraction (F);
- F: 100 μM aqueous solution of DMPO.

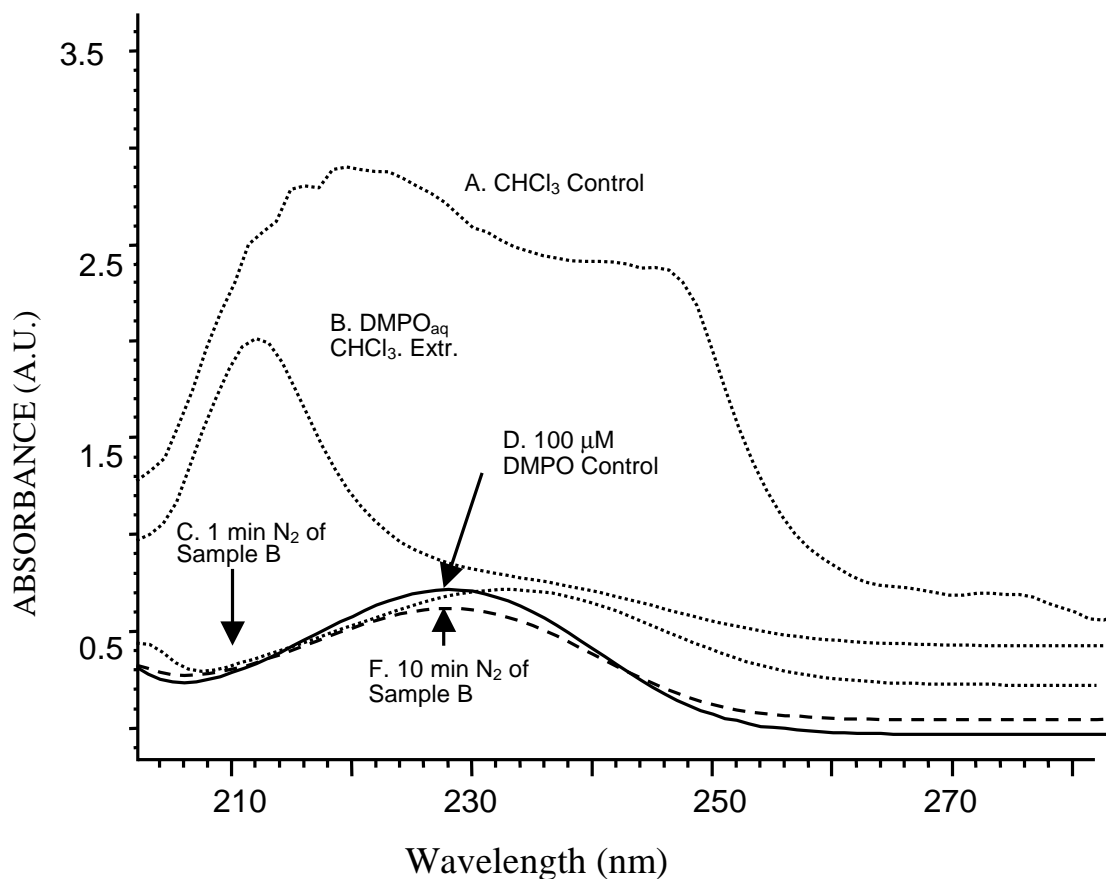


Figure 11. DMPO remains in the aqueous phase after CHCl_3 extraction. (UV spectra of DMPO $\epsilon_{225\text{nm}} \approx 7800 \text{ M}^{-1} \cdot \text{cm}^{-1}$ [Buettner GR, 1990]).

- A: CHCl_3 100 % control. Note, absorbance readings ≥ 2 are above the limits for reliability of the instrument;
- B: The UV spectrum of 100 μM aqueous solution of DMPO after CHCl_3 extraction ($\text{H}_2\text{O}/\text{CHCl}_3 = 1/2$ (v/v));
- C: Sample B purged with N_2 gas for 1 min. The difference in spectrum B and C demonstrates that the CHCl_3 that partitioned into the buffer is being purged by N_2 ;
- D: Sample B after purging with N_2 gas for 10 min; virtually all the CHCl_3 has been removed. The absorbance at 225 nm is comparable with the DMPO solution before extraction (E);
- E: 100 μM aqueous solution of DMPO.

Figure 12. The distribution of DMPO adduct of $\cdot\text{CH}_3$, $\cdot\text{OCH}_3$, and $\cdot\text{OOCH}_3$ after E.A. extraction. All spectra are from 12 signal-averaged scans collected over a total of 2 min and are representative of three different experiments.

- A: EPR spectrum of DMPO adducts formed by DMSO oxidation. The sample contains 50 mM DMPO, 100 mM DMSO, 100 μM H_2O_2 , and 50 μM Fe^{2+} ;
- B: Composite simulation using a ratio of 0.4:1.0:0.5 for C (DMPO/ $\cdot\text{CH}_3$), D (DMPO/ $\cdot\text{OCH}_3$), and E (DMPO/ $\cdot\text{OOCH}_3$), respectively;
- C: Simulated spectrum of DMPO/ $\cdot\text{CH}_3$: $a^{\text{N}} \approx 15.8$ G, $a^{\text{H}} \approx 22.6$ G, Linewidth ≈ 0.8 G, Lorentzian/Gaussian ≈ 1.0 ;
- D: Simulated spectrum DMPO/ $\cdot\text{OCH}_3$: $a^{\text{N}} \approx a^{\text{H}} \approx 14.8$ G, Linewidth ≈ 1.0 G, Lorentzian/Gaussian ≈ 0.7 ;
- E: Simulated spectrum of DMPO/ $\cdot\text{OOCH}_3$: $a^{\text{N}} 14.6$ G, $a^{\text{H}} \approx 14.6, 1.3$ G, Linewidth ≈ 1.0 G, Lorentzian/Gaussian ≈ 0.7 ;
- F: Sample A in aqueous phase after extraction;
- G: Sample A in E.A. phase after extraction.

A. DMSO oxidation, in PB suspension



B. Computer simulation: C:D:E = 0.8:1.0:0.3



C. DMPO/ $\dot{\text{C}}\text{H}_3$



D. DMPO/ $\dot{\text{O}}\text{C}\text{H}_3$



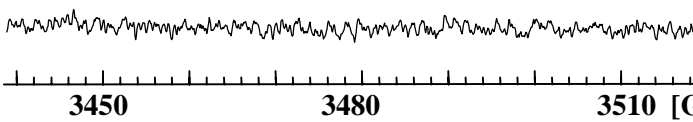
E. DMPO/ $\dot{\text{O}}\text{O}\text{C}\text{H}_3$



F. Sample A in aqueous phase



G. Sample A in E.A. phase



small molecular weight DMPO adducts will be remain in the aqueous phase after extraction.

Therefore, E.A. and Folch extraction ($\text{CHCl}_3/\text{MeOH}$) are suitable solvents for the extraction of lipid-derived radicals during oxidation of DHA, cell, and LDL models. We expect that extraction will improve the identification of DMPO spin adducts *via* their affinities for different solvents as well as their hyperfine splitting constants.

Extraction Increases Stability of DMPO Spin Adducts

To test our hypothesis that extraction will stabilize the lipid-derived DMPO spin adducts, we applied E.A. extraction to a lipid peroxidation experiment using DHA as the unsaturated lipid. As shown as Figure 13A, there are only two major radical species detected at 5 min after addition of ferrous iron when no extraction was applied. This EPR spectrum constantly changes as shown in Figures 5 and 9. Only 2-3 min were generally available to collect this particular EPR signal. Thus, the measurement of a temporary radical profile and gathering a high quality spectrum are impossible.

However, upon combining EPR with E.A. extraction, DMPO spin adducts were distributed between both the ethyl acetate and the aqueous phases (Figure 13 B-C) and were thereby greatly stabilized (> 10 h).

Stabilization of the radical adducts allows a longer time for signal averaging. Signal averaging improves the spectral signal-to-noise ratio, thereby improving the reliability of adduct identification.

Identification of the DMPO Adducts Post-Extraction

Figures 14 and 15 are examples that demonstrate the advantages of the extraction method over EPR spin trapping without extraction. The radical adducts can be identified not only *via* their hyperfine splitting constants, but also *via* their affinity for either water

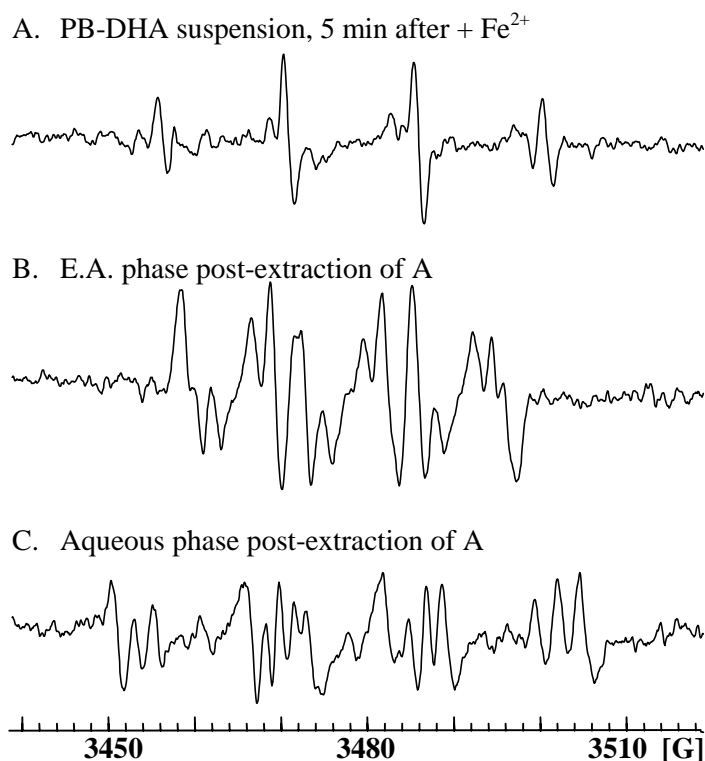


Figure 13. Extraction with E.A. increases the lifetime of DMPO adducts observed during DHA lipid peroxidation. The reaction system contained 5 mM DHA incubated with 50 mM DMPO, 55 μ M DTPA, 250 μ M O₂, and 50 μ M Fe²⁺. These spectra are representative of at least five different experiments.

- A: EPR scans were initiated 5 min after addition of Fe²⁺. The spectrum is constantly changing, refer to Figures 5 and 9. Thus, only a 2-3 min window is available to collect specific spectra; this short time limits the opportunity to signal-average data to enhance very weak EPR signals. This spectrum is the result of 12 signal-averaged scans collected over a total of 2 min;
- B: The lifetimes of spin adducts in the E.A. phase post-extraction are much longer (> 10 h) allowing signal-averaging techniques to be used to great advantage. This spectrum is the result of 120 signal-averaged scans collected over a total of 20 min of the E.A. phase;
- C: The lifetimes of spin adducts in the aqueous phase post-extraction are also much longer. This spectrum is the result of 120 signal-averaged scans collected over a total of 20 min of the aqueous phase.

Figure 14. Two DMPO adducts are observable in the organic phase (E.A.) after extraction in the DHA-peroxidizing system of Figure 13. A small amount of the low molecular weight spin adducts, such as DMPO/HO[•] and DMPO/HOO[•] can partition into the E.A. phase upon extraction with $a^N \approx 13.7$ G, $a^H \approx 10.4$ G; $a^N \approx 13.0$ G, $a^H \approx 10.5$, and 1.4 G, respectively. However, these adducts can be removed from the E.A. phase by complete evaporation using N₂-purging. This spectrum is representative of at least five different experiments.

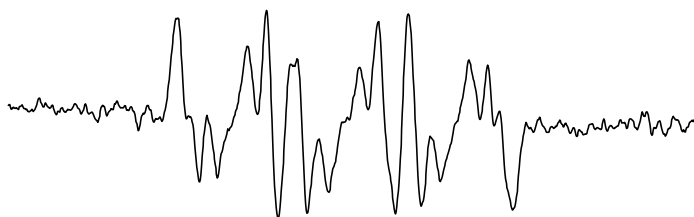
A: EPR spectrum in the E.A. phase of DHA oxidation system, *e.g.* Figure 13B;

B: Composite simulation using a ratio of 1.0:0.7 for the alkoxy radical adduct DMPO/LO[•] and peroxy radical adduct DMPO/LOO[•] or DMPO/OLOO[•], C and D respectively;

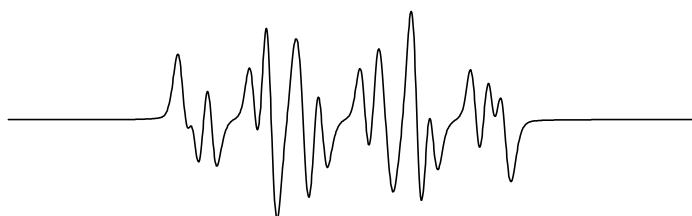
C: Simulated spectrum of DMPO/LO[•]: $a^N \approx 13.5$ G, $a^H \approx 10.2$ G, linewidth ≈ 1.3 G, Lorentzian/Gaussian ≈ 0.7 ;

D: Simulated spectrum of DMPO/LOO[•]: $a^N \approx 12.8$ G, $a^H \approx 6.85$ G; 1.9 G, linewidth ≈ 1.1 G, Lorentzian/Gaussian ≈ 0.5 .

A. E.A. phase post-extraction DHA



B. Computer simulation: C:D = 1:0.7



C. DMPO/LO[•]



D. DMPO/LOO[•] or DMPO/OLOO[•]

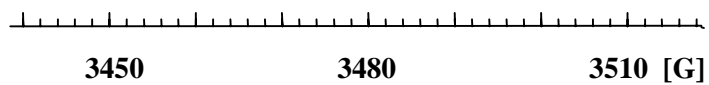
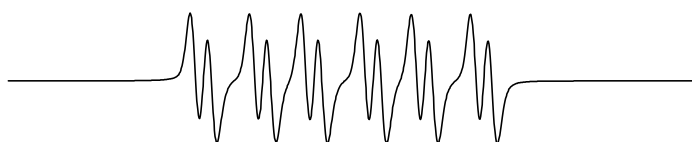


Figure 15. At least three DMPO adducts are clearly observed in the aqueous phase post-extraction in the DHA-peroxidizing system of Figure 13. There is also a hint of the presence of an unidentified three-line species (marked by * as 1:1:1 in A) that was not included in the computer analysis. This spectrum is representative of at least five different experiments.

A: EPR spectrum in the aqueous phase of DHA oxidation system, *e.g.* Figure 13C;

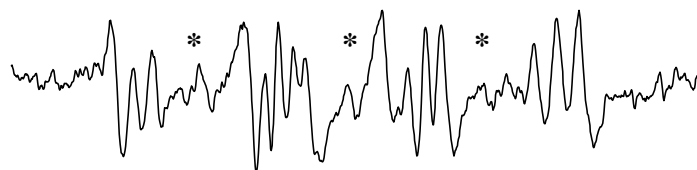
B: Composite simulation using a ratio of 0.4:1.0:0.5 for the two carbon-centered radical spin adducts (DMPO/C₁[•], DMPO/C₂[•]), and DMPO/RO[•] or DMPO/HO[•], for species C, D, and E respectively;

C: Simulated spectrum of DMPO/C₁[•]: $a^N_1 \approx 15.2$ G, $a^H_1 \approx 18.9$ G, Linewidth ≈ 0.8 G, Lorentzian/Gaussian ≈ 1.0 ;

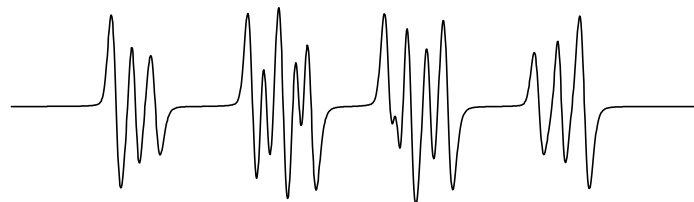
D: Simulated spectrum DMPO/C₂[•]: $a^N_2 \approx 15.8$ G, $a^H_2 \approx 22.6$ G, Linewidth ≈ 1.0 G, Lorentzian/Gaussian ≈ 0.7 ;

E: Simulated spectrum of RO[•]/HO[•]: $a^N \approx a^H \approx 14.8$ G, Linewidth ≈ 1.0 G, Lorentzian/Gaussian ≈ 0.7 .

A. Aqueous phase post-extraction of Figure 3A



B. Computer simulation: C:D:E = 0.4:1:0.5



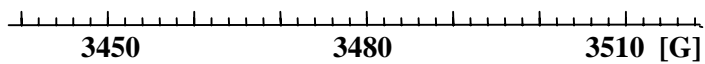
C. DMPO/C₁[•]



D. DMPO/C₂[•]



E. DMPO/RO[•] or DMPO/HO[•]



or organic solvent.

Species 1 ($a^N \approx 15.8$ G, $a^H \approx 22.6$ G)

As listed in Table 2, species 1 in the DHA suspension could have been a DMPO/R[•] adduct and/or a DMPO/L[•] adduct. In the previous section, we excluded DMPO/L[•] as species 1 based on kinetic considerations [Hasegawa K, 1978] rather than direct experiment evidence. The extraction method, for the first time, provides direct evidence for excluding L[•] as species 1. We know from Figure 12 that extraction separates the short chain radical adducts in the aqueous phase from the long chain radical adducts in the E.A. phase. The data of Figure 14-16 reveal that only short chain carbon-centered radicals (DMPO/R[•]) are in the aqueous phase; no long chain carbon-centered radical adducts (DMPO/L[•]) are observed in the ethyl acetate phase. Figure 15C shows the simulation of the DMPO/R[•] adduct. Thus, we assign species 1 to DMPO/R[•], which could not have been done experimentally without extraction.

Species 2 ($a^N \approx 15.2$ G, $a^H \approx 18.9$ G)

Using the extraction method, similar results for the identification of species 2 are observed. Without extraction two radical adducts, DMPO/OR[•] and DMPO/OL[•], could be assigned as species 2. The OR[•] is a radical derived from β -scission alkyl radicals. After extraction the DMPO/OR[•] adduct was only detected in the aqueous phase but not in the E.A. phase (Figure 14-16). Thus, we assign species 2 as DMPO/OR[•]. This assignment was also supported by computer simulation, Figure 15D.

Species 3 (1:2:2:1 $a^N \approx a^H \approx 14.8$ G)

Ethyl acetate extraction reveal that species 3 may consist of three radical adducts, DMPO/[•]OR, DMPO/[•]OL or DMPO/[•]OH, Figure 14-16. These spin adducts can have very similar hyperfine splitting constants [Kraiev AG, 1996; 1996]. The

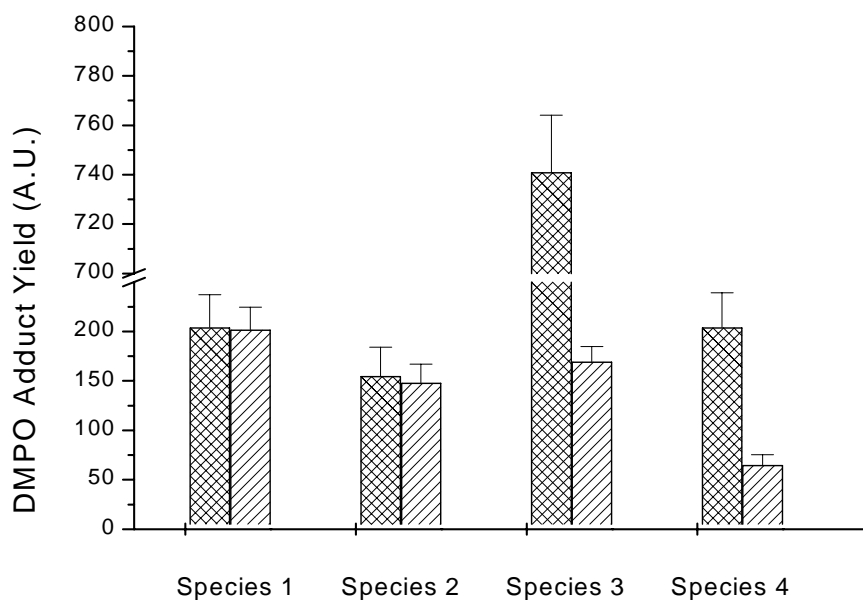


Figure 16. Comparison of DMPO adduct yield observed in the aqueous phase before and after E.A. extraction. The sample contained 5 mM DHA incubated with 50 mM DMPO, 250 μ M Fe^{2+} . Data were collected after addition of Fe^{2+} 5 min. 70 A.U. represents the EPR background noise level. In the bars, \times represents radical adduct yield in the suspension before extraction; $///$ represents radical adduct yield in the aqueous phase after extraction; $n = 3$. Error bars represent the standard deviation.

DMPO/•OR adduct should only be detected in the aqueous phase after extraction according to our previous experiments, Figure 12. The DMPO/•OL adduct was only found in the ethyl acetate phase. Thus, the difference between these two radical adducts can be easily distinguished *via* the extraction method.

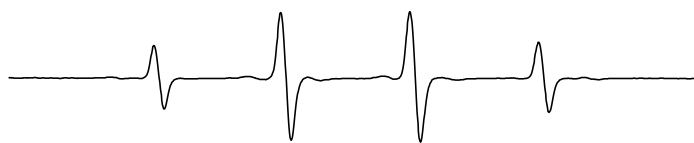
However, it is difficult to determine if species 3 should be assigned as the DMPO/•OH adduct. In Fe²⁺-mediated PUFA oxidation, DMPO/•OH could be formed by a non-radical mechanism [Hanna PM, 1992] or by O₂^{•-}-derived Fenton reaction [Chamulitrat W, 1991; Rota C, 1997]. It is not surprising to observe DMPO/•OH during DHA oxidation. The DMPO/•OH adduct could be distributed between both the aqueous and the organic phases after extraction [Schaich KM, 1990, Trudell JR, 1987]. This causes the problem of whether DMPO/•OL or DMPO/•OH adduct should be assigned as this species ($a^N \approx 13.5$ G, $a^H \approx 10.2$ G) in the E.A. phase.

To address this problem, we used a Fenton system as a means to generate authentic DMPO/•OH. The Fenton system consisted of 50 mM DMPO, 100 μM H₂O₂, and 50 μM Fe²⁺. Only the DMPO/•OH adduct is formed in this system. When the Fenton DMPO product was extracted, the spectrum observed (Figure 17B) is comparable to an adduct observed in DHA oxidation, Figure 14C. The hyperfine splitting constants of the DMPO/•OH in the ethyl acetate phase is $a^N \approx 13.6$ G, $a^H \approx 10.9$ G. However, DMPO/•OH in E.A. can be evaporated with N₂ purging as it is no longer observed when the residue is resuspended in 100% E.A, Figure 17C. Because DMPO is a highly volatile compound, it can be removed from the ethyl acetate phase with nitrogen purging. Likewise, because DMPO/•OH is quite small, it too will evaporate upon purging with nitrogen. Thus, species 3 can be assigned as aqueous adducts DMPO/•OH and DMPO/•OR in water; but, in E.A. this species ($a^N \approx 13.6$ G, $a^H \approx 10.9$ G) should be assigned as DMPO/•OL.

Figure 17. The distribution of DMPO/•OH and DMPO/•OOH after E.A. extraction. All spectra are from 12 signal-averaged scans collected over a total of 2 min and are representative of at least five different experiments.

- A: EPR spectrum of DMPO/•OH ($a^N \approx a^H \approx 14.8$ G) formed by the Fenton reaction in PB suspension. The sample contains 50 mM DMPO, 100 μ M H₂O₂, and 50 μ M Fe²⁺;
- B: EPR spectrum of DMPO/•OH ($a^N \approx 13.6$ G, $a^H \approx 10.9$ G) in E.A. phase after sample A was extracted;
- C: No radicals were observed when sample B was subjected to N₂-purging and then resuspended in E.A.;
- D: EPR spectrum of DMPO/•OOH ($a^N \approx 14.3$ G, $a^H \approx 11.6$ G, 1.2 G) formed from the reaction of HX (hypoxanthine)/XO (xanthine oxidase) in PB suspension. The sample contains 50 mM DMPO, 0.5 mM HX, and 0.1 U/mL XO;
- E: EPR spectrum of DMPO/•OOH ($a^N \approx 13.0$ G, $a^H \approx 10.5$ G, 1.4 G) in E.A. phase after sample D was extracted;
- F: No radicals were observed when sample E was subjected to N₂-purging and then resuspended in E.A.

A. DMPO/ $\dot{\text{O}}\text{H}$ in suspension



B. DMPO/ $\dot{\text{O}}\text{H}$ in E.A. post-extraction



C. Sample C re-suspended in E.A. post N_2 -purging



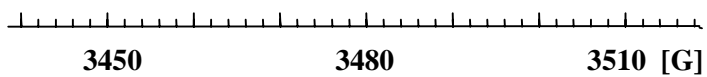
D. DMPO/ $\dot{\text{O}}\text{O}\text{H}$ in suspension



E. DMPO/ $\dot{\text{O}}\text{O}\text{H}$ in E.A. post-extraction



F. Sample E re-suspended in E.A. post N_2 -purging



Species 4 ($a^N \approx 14.6$ G; $a^H \approx 10.2, 1.3$ G)

There are four radical adducts (DMPO/ $\dot{\text{O}}\text{OH}$, DMPO/ $\text{ROO}\dot{\text{O}}$, DMPO/ $\text{LOO}\dot{\text{O}}$, DMPO/ $\text{OLOO}\dot{\text{O}}$) that could possibly be assigned to this species based on the observed hyperfine splitting constants. After extraction, there was no detectable signal with this hyperfine splitting in the aqueous phase (Figure 15 and 16). Thus, species 4 possibly consists of two long chain radical adducts, DMPO/ $\text{LOO}\dot{\text{O}}$ and DMPO/ $\text{OLOO}\dot{\text{O}}$, as well as DMPO/ $\dot{\text{O}}\text{OH}$.

Like DMPO/ $\dot{\text{O}}\text{H}$ adduct, DMPO/ $\dot{\text{O}}\text{OH}$ is another radical adduct that can be distributed in both the aqueous and E.A. phases after extraction. To specify DMPO/ $\dot{\text{O}}\text{OL}$ or DMPO/ $\dot{\text{O}}\text{OH}$ in the assignment of species 4, we did a control experiment using the reaction of HX (hypoxanthine)/XO (xanthine oxidase) in PB suspension to produce the superoxide radical. The reaction mixture contained 50 mM DMPO, 0.5 mM HX, and 0.1 U/mL XO and was extracted with ethyl acetate, Figure 17 D-F. The DMPO/ $\dot{\text{O}}\text{OH}$ signal in E.A. phase (Figure 17E) disappeared after the sample of 17E was purged with N_2 and resuspended in 100% E.A. (Figure 17F). Thus, we suggest that DMPO/ $\dot{\text{O}}\text{OH}$ is not a part of species 4; it seems that species 4 consists of only long chain radicals, e.g. DMPO/ $\text{LOO}\dot{\text{O}}$ and DMPO/ $\text{OLOO}\dot{\text{O}}$.

These results demonstrate that extraction can greatly aid in the identification of radical species. It stabilizes DMPO adducts for EPR spectroscopy. It also helps us to separate adducts by their hydrophilic/hydrophobic properties. This separation, when coupled with hyperfine splitting constants, can aid in the correct assignment of spin adducts.

Radical Profile Determined by EPR-Extraction

Using EPR-extraction, we are able to observe the time profile of adduct formation during in DHA oxidation. Figure 18 shows the lipid radicals formed during Fe^{2+} -mediated

Figure 18. The profile of lipid-chain radical adduct (DMPO/OLOO[•] or DMPO/LO[•]) determine by an EPR-Extraction. DHA oxidation system contains: 5 mM DHA, 50 mM DMPO, 100 μ M Fe²⁺. Five mL E.A. was used to extract lipid and lipid radical into E.A. at various time points. All spectra are from 12 signal-averaged scans collected over a total of 20 min and are representative of at least three different experiments.

A: E.A. extraction was applied at 20 s after addition of Fe²⁺;

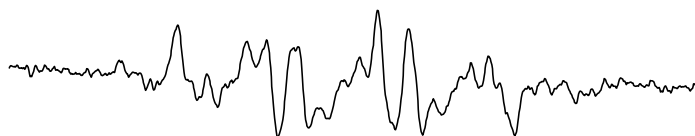
B: E.A. extraction was applied at 40 s after addition of Fe²⁺;

C: E.A. extraction was applied at 1 min after addition of Fe²⁺;

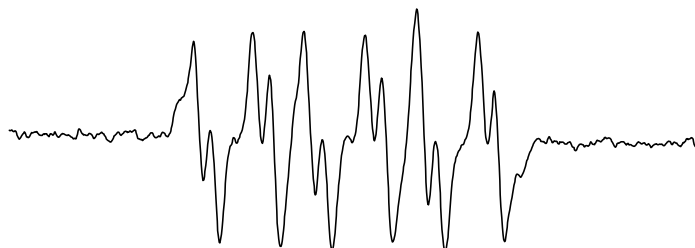
D: E.A. extraction was applied at 15 min after addition of Fe²⁺;

E: E.A. extraction was applied at 1 h after addition of Fe²⁺.

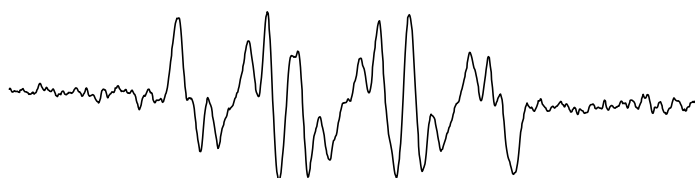
A. E.A. extraction at 20 s after Fe^{2+}



B. E.A. extraction at 40 s after Fe^{2+}



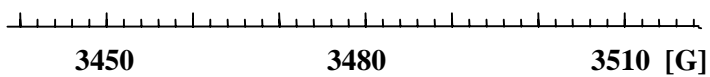
C. E.A. extraction at 5 min after Fe^{2+}



D. E.A. extraction at 15 min after Fe^{2+}



F. E.A. extraction at 1 h after Fe^{2+}



DHA oxidation at different time points. The radical profile can be determined at any specific time point *via* a simple extraction procedure. After extraction there are no actual time limitations for the gathering of EPR spectra. It is interesting to note that the lipid-derived radicals observed, especially, lipid peroxy radicals, correlate well with the oxygen consumption experiment (Figure 8). The production of lipid peroxy radicals approaches its highest yield about 40 s after the addition of Fe^{2+} .

Summary of EPR-Extraction

Compared to simple EPR spin trapping in suspension, our EPR-extraction protocol has many advantages. The stability of DMPO adducts is greatly improved by extraction. Due to the longer lifetime of DMPO adducts post-extraction, it is possible to do signal-averaging over a longer time to generate spectra of good enough quality that assignment of radical species could be better accomplished. The distribution of spin adducts between the phases after extraction allows us also distinguish radical adducts *via* their varied hydrophilic/hydrophobic natures, in addition to their hyperfine spin splitting constants.

Two species (species 3, and 4) in the aqueous phase are fully or partially extracted into the E.A. phase. This indicates that these two species in the aqueous phase belong to lipid chain radicals, e.g. lipid oxygen-centered radicals (LO^\bullet and LOO^\bullet or OLOO^\bullet). The difference in the hyperfine constants between these two species in the E.A. phase suggests that they are two different types of lipid chain radicals. Thus, rather than assigning species 4 as organic alkoxyl radicals [Dikalov S, 1999], we suggest that species 4 should be assigned to lipid oxygen-centered radicals (LO^\bullet and LOO^\bullet or OLOO^\bullet), which originally results from species 3 and 4, and are detected in the E.A. phase using our extraction protocol, Figure 14. The small fragment radicals (R^\bullet , HO^\bullet , RO^\bullet) will be mostly present in the aqueous phase (Figure 15) after extraction.

DEPMPO in a DHA Study

DEPMPO (5-diethoxyphosphoryl-5-methyl-1-pyrroline-*N*-oxide), a cousin of DMPO, is a new nitron compound that has been recently used in EPR spin trapping to detect a variety of free radicals, especially oxygen-centered radicals in biological systems [Frejacille C, 1995; Lui KJ, 1999]. DEPMPO has a chemical structure nearly identical to DMPO (Table 1) except a phosphate group is on the pyrroline ring. They both can efficiently trap carbon-centered and oxygen-centered radicals. However, DEPMPO has a number of advantages compared to DMPO. It was reported that DEPMPO has improved stability for the superoxide spin adduct [Tuccio B, 1995, Frejaville C, 1995]; its half-life is 15-times longer than that of DMPO/*OOH. It has also been reported that DEPMPO has a high efficiency for trapping superoxide [Roubaud V, 1997]. In addition, there is no significant decomposition reaction of DEPMPO/*OOH to DEPMPO/*OH observed in phosphate buffered saline (PBS) [Roubaud V, 1998].

Due to the phosphate group, DEPMPO is even more hydrophilic than DMPO. Thus, DEPMPO should be highly suitable for use in the EPR-extraction experiments. As with the DMPO study, we expected that the extraction process will separate unreacted DEPMPO and the oxidation mediator (iron) from the oxidizable substrate (unsaturated lipid), thereby slowing or stopping the lipid peroxidation cycle, and thus slowing the reactions that destroy the DEPMPO adduct (reaction 21).



Consequently, DEPMPO adducts will be distributed into different phases and thus be stabilized after extraction. By separating the spin adducts with extraction, we expect to be able to identify the radicals not only by their hyperfine-splitting constants, but also by their hydrophilic or hydrophobic nature.

Using DEPMPO as spin trap, three species (Figure 19A and B) are usually detected by EPR in a DHA aerobic suspension. Comparing our experimental data with published values [NIH spin trapping data base, Frejaville C, 1995, Lui KJ, 1999], we identified one carbon-centered radical ($a^P_A \approx 48.9$ G, $a^N_A \approx 14.7$ G, $a^H_A \approx 21.3$ G) and two oxygen-centered radicals ($a^P_B \approx 47.1$ G, $a^H_B \approx a^N_2 \approx 13.7$ G; $a^P_B \approx 50.1$ G, $a^N_C \approx 12.9$ G, $a^H_C \approx 11.3$ G). All of these species were found to have much longer lifetimes than their related DMPO adducts. For example, the DMPO adduct species 4 of Figure 1 has a half-life of 1-2 min, while its related DEPMPO adduct, species C in Figure 19C, has a half-life of more than 5 min.

As shown as Figure 19A, the EPR spectrum of DEPMPO adducts is usually viewed as two identical parts in 3400-3550 G magnetic field because of a large spin splitting of the phosphorus atom (about 50 G) present in DEPMPO. To simplify the analysis of the EPR spectrum and to save time for signal-averaging, only the lower magnetic field part of the spectrum (3420-3495 G) is viewed for most of our EPR observations, Figure 19B.

DEPMPO Study and E.A. Extraction

We used our extraction procedure with DEPMPO as the spin trap in a DHA oxidation system; improved stability of the EPR spectra can be achieved, similar to the DMPO extraction study. Figure 20A shows a constantly changing spectrum that is usually observed in a suspension system; only 2-5 min need be used to collect this particular signal. However, applying E.A. extraction, DEPMPO adducts are distributed in both aqueous and E.A. phases, thereby being stabilized (Figure 20B and D). The longer lifetime of the adducts post-extraction provides additional information on the radicals, which is available in a suspension study (Figure 20A). For example, in Figure 20A species A appears to be only one radical adduct but after extraction, two radical

Figure 19. EPR spectra of DEPMPO/L_d• formed by Fe²⁺-mediated DHA oxidation. The sample contains 16 mM DEPMPO, 5 mM DHA, 60 μM DTPA, and 50 μM Fe²⁺. There are three species observed in this time period (5 min after Fe²⁺). The spectra are representative of at least five different experiments.

A: EPR spectrum of DEPMPO/L_d• viewed with the full range of the magnetic field (3400 G-3550G). The spectrum is derived from 6 signal-averaged scans collected over a total of 4 min;

B: EPR spectrum of DEPMPO/L_d• was viewed with magnetic field from 3220 G-3495 G. The spectrum is from 6 signal-averaged scans collected over a total of 2 min;

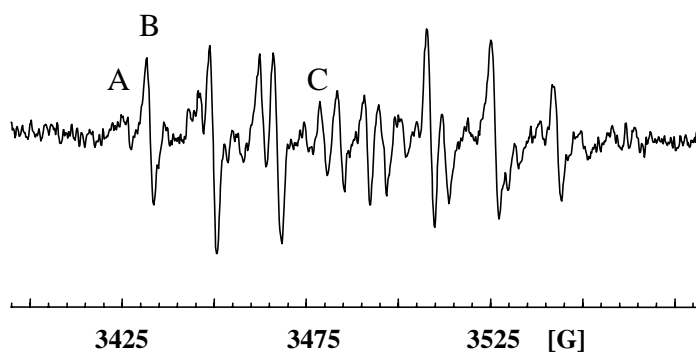
C: Composite simulation using a ratio of 0.2:1:0.4 for species A:B:C, respectively; Linewidth ≈ 1.0 G, Lorentzian/Gaussian ≈ 1.1;

D: Computer simulation of species A: $a^P \approx 48.9$ G, $a^N \approx 14.7$ G, $a^H \approx 21.3$ G;

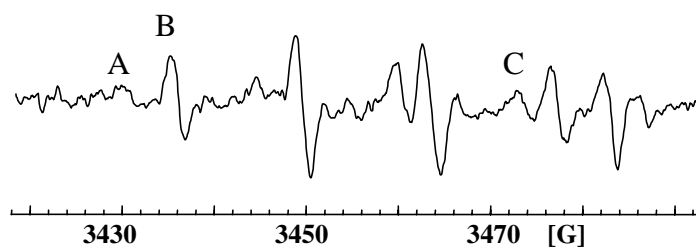
E: Computer simulation of species B: $a^P \approx 47.1$ G, $a^N \approx a^H \approx 13.7$ G;

F: Computer simulation of species C: $a^P \approx 50.1$ G, $a^N \approx 12.9$ G, $a^H \approx 11.3$ G.

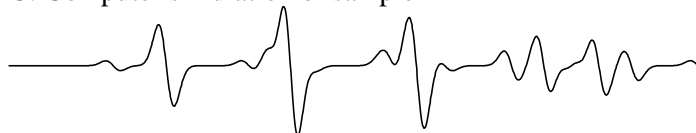
A. A full view EPR spectrum of DEPMPO adducts



B. A partial view EPR spectrum of DEPMPO adducts



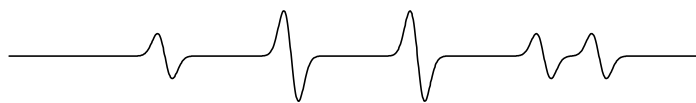
C: Computer simulation of sample B



D: Computer simulation of species A



E: Computer simulation of species B



F: Computer simulation of species C



Figure 20. Extraction with E.A. increases the lifetime of DEPMPO adducts observed during DHA lipid peroxidation. The reaction system contains 16 mM DEPMPO, 5 mM DHA, 60 μ M DTPA, and 50 μ M Fe^{2+} . The spectra are representative of at least three different experiments.

A: EPR spectrum of DEPMPO adducts formed from a suspension system. The spectrum is derived from 6 signal-averaged scans collected over a total of 2 min;

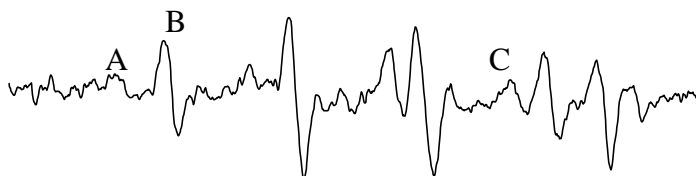
B: the lifetimes of spin adducts in the aqueous phase post-extraction are much longer allowing signal averaging techniques to be used to great advantage. This spectrum of the aqueous phase is the result of 60 signal-averaged scans collected over a total of 20 min. Three radical adducts are observed. They are species A, B and an additional species;

C: Computer simulation of the additional carbon-centered radical ($a^{\text{P}} \approx 46.0$ G, $a^{\text{N}} \approx 14.5$ G, $a^{\text{H}} \approx 19.8$ G) that was detected in the aqueous phase after extraction, but was not distinguishable in the suspension system;

D: the lifetimes of spin adducts in the E.A. phase post-extraction are much longer allowing signal averaging techniques to be used to great advantage. This spectrum of the E.A. phase is the result of 60 signal-averaged scans collected over a total of 20 min. There are at least two lipid-chain radical adducts, (E and F) in this spectrum;

E: Composite simulation of DEPMPO/ HO^{\bullet} in a partial view: ($a^{\text{P}} \approx 47.5$ G, $a^{\text{N}} \approx 13.0$ G, $a^{\text{H}} \approx 12.0$ G) and (DEPMPO/ HOO^{\bullet} : $a^{\text{P}} \approx 48.9$ G, $a^{\text{N}} \approx 11.8$ G, $a^{\text{H}} \approx 10.5$ G) in E.A. There is a significant difference between D and E, suggesting that D is due to the lipid radical adducts rather than from other mechanisms such as non-radical pathways.

A: DHA suspension, 5 min after Fe^{2+}



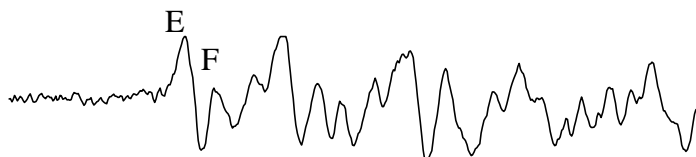
B: Aqueous phase post-extraction of A



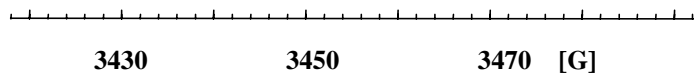
C: An additional carbon-centered radical



D. E.A. phase post-extraction of A



E. Composite simulation of $\text{DEPMPO}/\cdot\text{OH}$, and $\text{DEPMPO}/\cdot\text{OOH}$



adducts can be identified (Figure 20B). Comparing the experimental data with published values, these two species can be assigned as carbon-centered radical adducts because they have the hyperfine splitting constants: ($a^P \approx 48.9$ G, $a^N \approx 14.7$ G, $a^H \approx 21.3$ G) and ($a^P \approx 46.0$ G, $a^N \approx 14.5$ G, $a^H \approx 19.8$ G). In addition, they are hydrophilic which restricts their observation in the E.A. phase, Figure 20D.

After extraction, species B ($a^P \approx 47.1$ G, $a^N \approx a^H \approx 13.7$ G) distributed partially in the aqueous phase and partially in the E.A. phase (Figure 20B and D). We propose that species B in Figure 20A might contain two types of radicals. As we concluded in the DMPO study, the species ($a^P \approx 47.1$ G, $a^N \approx a^H \approx 13.7$ G) that remains in the aqueous phase was assigned to either DEPMPO/ $\dot{O}H$ formed from a non-radical pathway, or DEPMPO/ $\dot{O}R$ derived from β -scission pathway. This species partitions into the E.A. phase similar to species E, which was proposed to be a lipid-chain radical. There is no detectable signal from species C in the aqueous phase after extraction (Figure 20B). In fact, species C completely partitions into the E.A. phase; thus, it is identified as another lipid-chain radical, *i.e.* species F in the E.A. phase (Figure 20D).

There are other species that can partition into E.A. that have hyperfine splitting constants similar to species E and F, *e.g.* DEPMPO/ $\dot{O}H$ and DEPMPO/ $\dot{O}OH$. To avoid misassignment of them as species E and F, we examined the behavior of DEPMPO/ $\dot{O}H$ (Figure 21B) and DEPMPO/ $\dot{O}OH$ (Figure 21E) in E.A. extraction the same way we did in the DMPO study. As shown as Figure 21, a fraction of DEPMPO/ $\dot{O}H$ and DEPMPO/ $\dot{O}OH$ can be detected in the E.A. phase. However, they disappear upon the N_2 -purging and E.A. resuspension process. Furthermore, the composite simulation of DEPMPO/ $\dot{O}H$ and DEPMPO/ $\dot{O}OH$ in E.A. (Figure 21H, *e.g.* 19E) shows significantly different spectra as compared to spectrum 20D. Thus, Figure 20D should be assigned to the lipid radical adducts: DEPMPO/ $LOO\dot{O}$ and DEPMPO/ $LO\dot{O}$.

Figure 21. The distribution of DEPMPO/ $\dot{\text{O}}\text{H}$ and DEPMPO/ $\dot{\text{O}}\text{O}\text{H}$ during our extraction procedure. Spectra A and E are derived from 6 signal-averaged scans collected over a total of 4 min. Others are the result of 12 signal-averaged scans collected over a total of 8 min. The spectra are representative of at least three different experiments.

- A: EPR spectrum of DEPMPO/ $\dot{\text{O}}\text{H}$ ($a^{\text{P}} \approx 47.4$ G, $a^{\text{N}} \approx 14.0$ G, $a^{\text{H}} \approx 13.0$ G) formed by the Fenton reaction in PB suspension. The sample contains 50 mM DMPO, 100 μM H_2O_2 , 50 μM Fe^{2+} , and 55 μM DTPA;
- B: EPR spectrum of DEPMPO/ $\dot{\text{O}}\text{H}$ in E.A. ($a^{\text{P}} \approx 47.0$ G, $a^{\text{N}} \approx 13.0$ G, $a^{\text{H}} \approx 12.0$ G) after sample A was extracted;
- C: No radicals were observed when sample B was subjected to N_2 -purging and then resuspended in E.A.;
- D: EPR spectrum of DEPMPO/ $\dot{\text{O}}\text{O}\text{H}$ ($a^{\text{P}} \approx 48.5$ G, $a^{\text{N}} \approx 13.2$ G, $a^{\text{H}} \approx 10.3$ G) formed from the reaction of HX (hypoxanthine)/ XO (xanthine oxidase) in PB suspension. The sample contains 50 mM DMPO, 0.5 mM HX, and 0.5 U/mL XO;
- E: EPR spectrum of DEPMPO/ $\dot{\text{O}}\text{O}\text{H}$ ($a^{\text{P}} \approx 48.2$ G, $a^{\text{N}} \approx 11.8$ G, $a^{\text{H}} \approx 10.5$ G) in E.A. phase after sample D was extracted;
- F: No radicals were observed when sample E was subjected to N_2 -purging and then resuspended in E.A.;
- G: Composite simulation of DEPMPO/ $\text{HO}\dot{\text{O}}$ in a full view: $a^{\text{P}} \approx 47.5$ G, $a^{\text{N}} \approx 13.0$ G, $a^{\text{H}} \approx 12.0$ G) and (DEPMPO/ $\text{HOO}\dot{\text{O}}$: $a^{\text{P}} \approx 48.9$ G, $a^{\text{N}} \approx 11.8$ G, $a^{\text{H}} \approx 10.5$ G) in E.A.

A. DEPMPO[•]OH in suspension



B. DEPMPO[•]OH in E.A.



C. No DEPMPO[•]OH is observed after re-suspension



D. DEPMPO[•]OOH in suspension



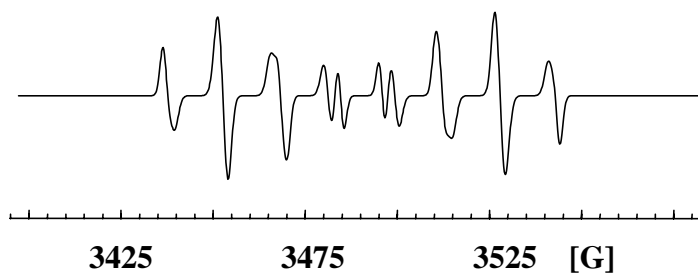
E. DEPMPO[•]OOH in E.A.



F. No DEPMPO[•]OOH is observed after re-suspension



G. Composite simulation of B and C.



Using DEPMPO in the DHA oxidation study, its adducts of oxygen-centered radicals were found to be much more stable than these adducts in the DMPO study. We hypothesized that even without extraction, DEPMPO adducts of oxygen-centered adducts would be stable enough to directly reflect the nature and structure of L^{\bullet}_d .

Define the Lipid Peroxyl-Type Radicals

According to the current thinking, $OLOO^{\bullet}$ is a major propagator among the other propagators in lipid peroxidation, Scheme 1. But until now, direct evidence of the formation of $OLOO^{\bullet}$ has not been reported. In our EPR studies, the extraction method provides a way to distinguish radicals *via* their hydrophilic or hydrophobic nature in addition to their hyperfine splitting constants. For the first time, we have used EPR-extraction to detect lipid peroxyl-type radicals, either $OLOO^{\bullet}$ or LOO^{\bullet} , in lipid peroxidation. However, we can not specifically identify each of them because both radical adducts are hydrophobic and have similar hyperfine splitting constants.

We found that the O_2 consumption of the DHA system varies considerably with the oxidation status of the DHA (Table 3). The oxidation status of DHA can either be varied by the 'storage time' of DHA or by exposure to air. In our experiments, the oxidation status of DHA, which had been stored longer than six months, can be approached by exposure of an unoxidized-DHA (newly open, < 2 week) to room air for 16-24 h. In these samples, LOOHs are formed by autoxidation of PUFA.

In experiments with oxidized-DHA, the pre-existing LOOH will react with Fe^{2+} to form LO^{\bullet} in the absence of oxygen (Figure 22A). The production of the LO^{\bullet} adduct (species B) will increase with increasing pre-exposure time of DHA to air (data not shown). Thus, more $OLOO^{\bullet}$ adduct can be formed during Fe^{2+} -oxidation of oxidized-DHA as compared to unoxidized-DHA. Indeed, we observed a significant difference in the intensity of species C in DHA that is peroxidized to different degrees, Figure 22C-G.

Table 3. Different oxidized status of DHA causes different O₂ depletion

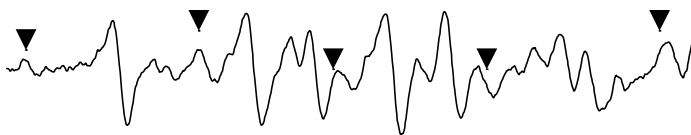
Oxidation Model	O ₂ Consumption Within first 1 min	O ₂ Consumption rate From 1 min to 3 h
PB only	26.3 ± 3.8 μM (35 s)	0.52 ± 0.054 μM/min
Oxidized DHA (stored > 6 month)	Without ST	60.4 ± 4.2 μM
	With ST	62.1 ± 5.3 μM
Oxidized DHA (air exposure 24 h)	Without ST	55.9 ± 6.2 μM
	With ST	58.1 ± 5.5 μM
Unoxidized DHA	42.3 ± 3.7 μM	1.44 ± 0.32 μM/min

Note: All experiments were done in an air-saturated suspension system which contained 1.25 mM DHA, 250 μM O₂, 50 mM Fe²⁺, with/without 16 mM DEPMPO. Data are expressed as means ± sd from n = 3. For the PB control experiment, O₂ is consumed fast. Thus, the first time period of O₂ consumption is for 35 s, not 1 min. ST represents spin trap, DEPMPO.

Figure 22. DEPMPO adducts observed during DHA lipid peroxidation. The reaction system contains 16 mM DEPMPO, 5 mM DHA (oxidized- or unoxidized), 60 μM DTPA, and 50 μM Fe^{2+} . The spectra are representative of at least three different experiments.

- A: EPR spectrum of DEPMPO adducts formed from an anaerobic suspension system. The spectrum is derived from 6 signal-averaged scans collected over a total of 2 min. There is an unknown species marked by ▼;
- B: Computer simulation of spectrum A using species A and B \approx 1.0:0.6.
- C: EPR spectrum of DEPMPO adducts formed from an aerobic DHA (oxidized-form) suspension system 1 min after Fe^{2+} was introduced;
- D: Composite simulation of spectrum C, which has contributions from species A, B, and C;
- E: EPR spectrum of DEPMPO adducts formed from an aerobic DHA (oxidized-form) suspension system 5 min after Fe^{2+} was introduced;
- F: EPR spectrum of DEPMPO adducts formed from an aerobic DHA (unoxidized-form) suspension system 5 min after Fe^{2+} was introduced;
- G: EPR spectrum of DEPMPO adducts formed from an aerobic (unoxidized-form) suspension system 30 min after Fe^{2+} was introduced.

A. DHA in anaerobic oxidation, 5 min after Fe^{2+}



B. Composite simulation: 5 min after Fe^{2+}



C. Oxidized DHA, 1 min after Fe^{2+}



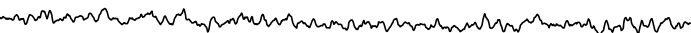
D. Composite simulation of C:



E. Oxidized DHA, 5 min after Fe^{2+}



F. Unoxidized DHA, 5 min after Fe^{2+}



G. Unoxidized DHA, 30 min after Fe^{2+}



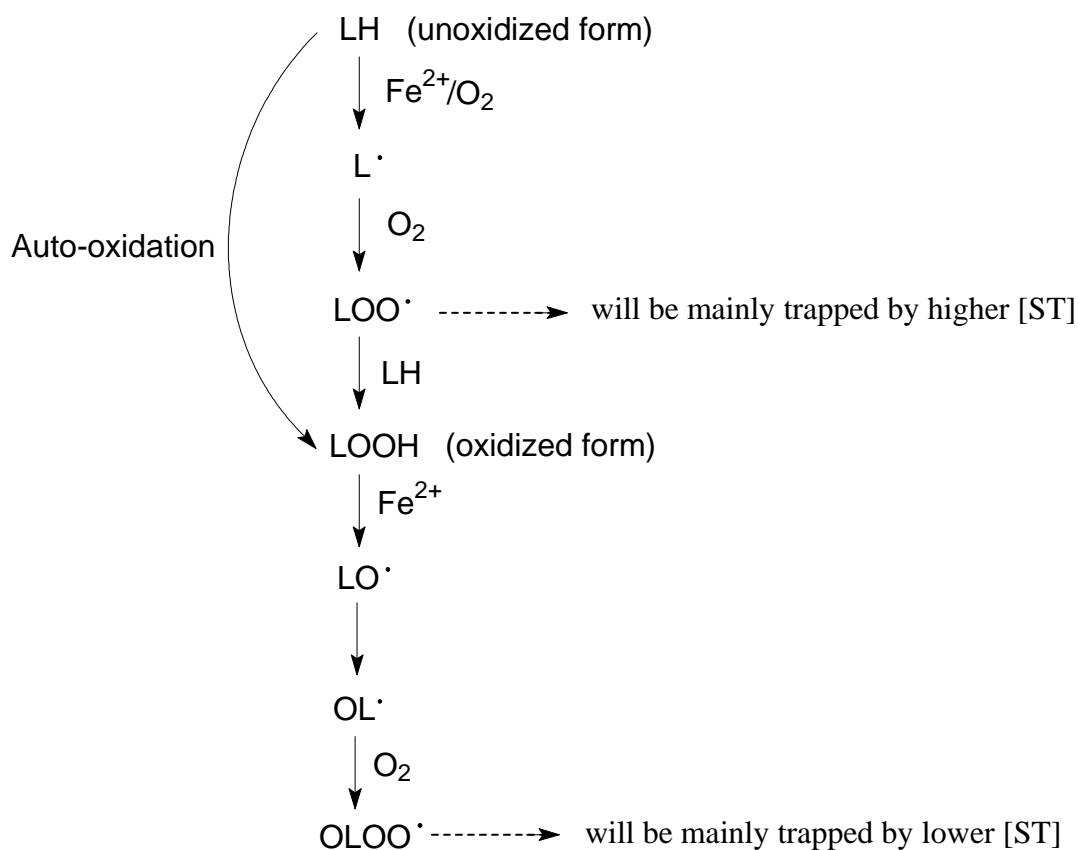
3425 3475 3525 [G]

Upon initiation of the oxidation of LH (unoxidized-DHA), LOO^\bullet will be the major product compared to OLOO^\bullet . In addition low $[\text{O}_2]$ should minimize the formation of OLOO^\bullet . During oxidation of unoxidized DHA, LOO^\bullet would be formed in the early stages (Scheme 4) and thus its adduct would be observed in the early stages when the rate of oxygen consumption is high (< 1 min, Table 3). However, in an experiment with unoxidized-DHA, species C was not detected at all, Figure 22F-G. To explain this, OLOO^\bullet rather than LOO^\bullet should be assigned as the lipid-peroxyl type radical trapped by DEPMPO. In addition, by comparing the experiments of oxygen depletion between systems with and without addition of DEPMPO (Table 3), we find that addition of DEPMPO did not inhibit the oxygen-depletion profile during the first stage of oxygen consumption, but it always greatly reduced the rate of oxygen-consumption after this period. These data indicate that LOO^\bullet is not the major species being trapped.

To make an assignment of species C, we also studied the relation of radical product vs. $[\text{DEPMPO}]$ in the unoxidized-DHA model. According to Scheme 4, LOO^\bullet would be formed before OLOO^\bullet . From a kinetic point of view, at a high spin trap concentration, LOO^\bullet will mainly be trapped, while at a low spin trap concentration OLOO^\bullet will mainly be trapped. However, as shown as Figure 23, as $[\text{DEPMPO}]$ varies from 8 to 64 mM, we see an opposite result. Increasing $[\text{DEPMPO}]$ in DHA oxidation always results in less of species C when the EPR measurement was done 30 min after treatment with iron. These data are consistent with our conclusion that species C is OLOO^\bullet rather than LOO^\bullet .

Summary of the DEPMPO Study

The lifetime of DEPMPO spin adducts observed post-extraction increased from min to h. However, the difficulty of assigning the lipid radical adducts in the E.A. phase greatly diminishes the usefulness of the EPR-extraction process with this spin trap. As



Scheme 4. Outline of the mechanism of lipid peroxidation of DHA. There is a different pathway if DHA oxidation starts with oxidized DHA or unoxidized DHA. Note, $\text{LOO}\cdot$ is formed early in the chain reaction, while $\text{OLOO}\cdot$ is formed later.

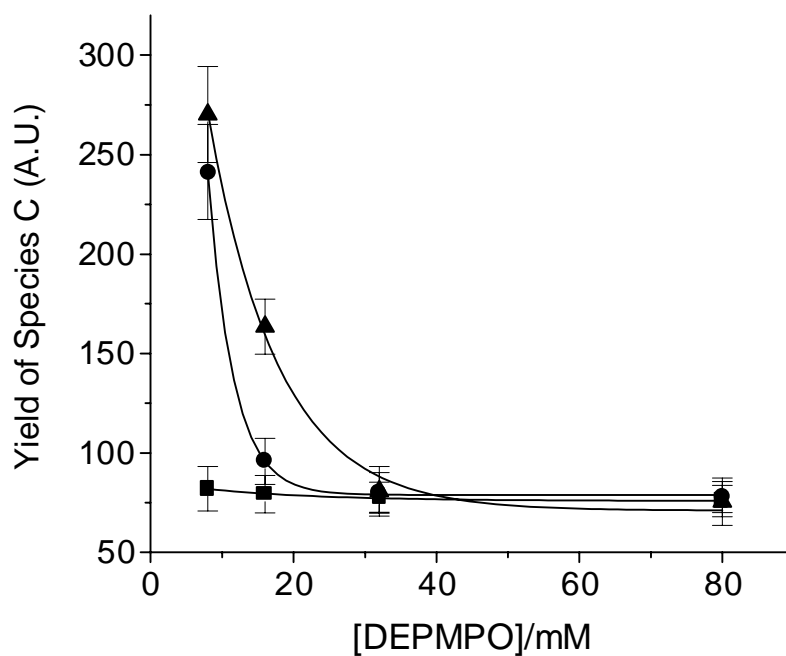


Figure 23. The relation of species C, e.g. peroxy-type radical and [DEPMPO]. The sample contains 5 mM unoxidized-DHA, with varying concentrations of spin trap, [DEPMPO]. The free radical chain reaction is initiated by addition of ferrous iron (50 μM). In the Figure, ● represents the yield of 30 min after addition of ferrous iron (50 μM); ▲ represents the yield of 60 min after addition of ferrous iron (50 μM); and ■ represents the yield of 5 min after addition of ferrous iron (50 μM). The DEPMPO adduct yield is represented as the EPR signal height from 12 signal-averaged scans collected over a total of 2 min, $n = 3$. Error bars represent standard deviation.

we can see, species C in Figure 19 and the two lipid radical adducts detected in the E.A. phase are too similar in their hyperfine structure. The DEPMPO study confirms our findings from the DMPO study that both radical profiles were comparable to the peroxy-type radical with DEPMPO. However, no extraction was needed due to the long lifetime of the DEPMPO adduct. Correlating the profile of the DEPMPO adduct with oxygen consumption, we found two types of peroxy radicals. We suggest that OLOO[•] rather than LOO[•] is the lipid peroxy radical that has been detected in our EPR study.

CHAPTER IV

EPR STUDY OF LIPID PEROXIDATION IN CELLS AND LDL

Using POBN as a spin trap, EPR has successfully been used to detect lipid-derived radicals from cells undergoing lipid peroxidation [Wagner BA, 1993; 1994; Buettner GR, 1993; Qian SY, 1999]. The production of POBN adducts during cellular lipid peroxidation correlates well with cell membrane damage as measured by the TBAR assay and Trypan blue dye exclusion [Kelley EE, 1997; Wagner BA, 1998; Schafer FQ, 1999]. POBN successfully traps only carbon-centered radicals (R^\bullet) derived from β -scission of lipid alkoxy radicals (LO^\bullet) and not oxygen-centered radicals. Thus, studies using POBN provide only partial information about lipid peroxidation in the cell membrane. It is thought that the radicals derived from β -scission play only a minor role in the propagation reactions of lipid peroxidation.

Unlike carbon-centered radicals, the oxygen-centered radicals, especially peroxy radicals, are the most reactive species involved in many radical chain reactions. To understand their role in lipid peroxidation, their detection is very important. It has been reported that peroxy radicals disproportionate at nearly diffusion-controlled rates [Bennett JEJ, 1987]. Thus, the study of the importance of peroxy radicals in biological systems is limited by their short lifetime; even their spin adducts have very short lifetime [Howard JA, 1978; Janzen EG, 1990; Dikalov S, 1999]. We have developed a method that increases their lifetimes and thus increases EPR ability to study these radicals.

In our DHA studies (Chapter 3), we established extraction techniques to assist in the successful EPR spin trapping of unstable radical adducts. Extraction stabilizes the

spin adducts, especially the oxygen-centered lipid radical adducts in the organic phase. Using this method, temporal profiles of radical formation can now be obtained (see Figure 18).

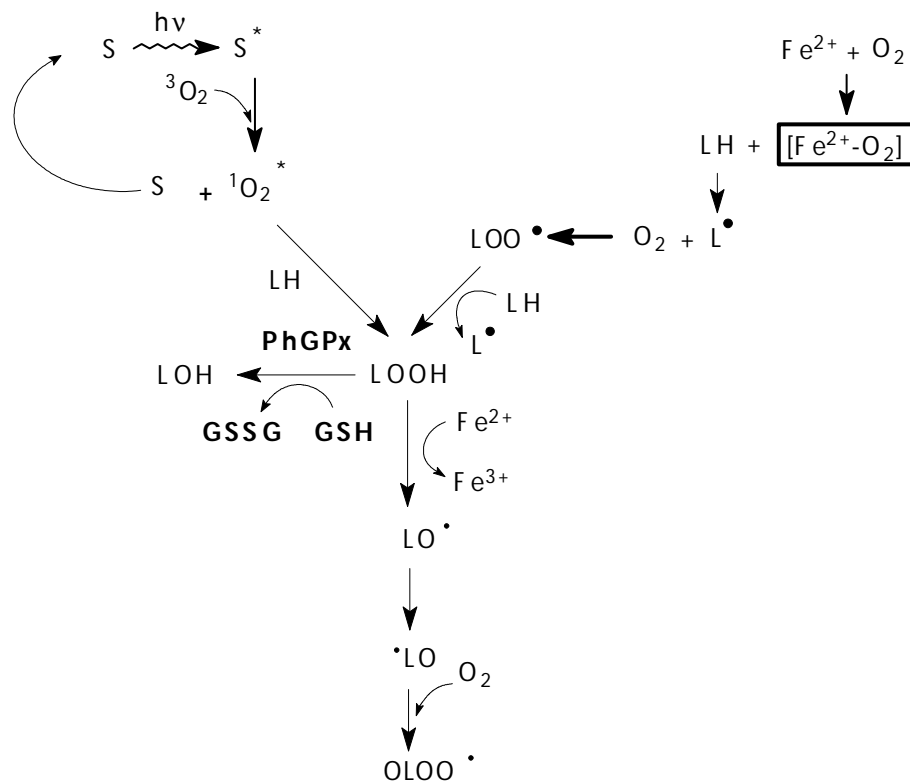
In this chapter, we use our newly developed extraction technique to study lipid peroxidation in cells and LDL samples. PUFAs in cell membranes are a part of the lipid structure. Most lipids in cell membranes are triglycerols with a phosphate moiety as a polar head group; also, the two hydrocarbon tails have varying unsaturation. Thus, the lipid is amphipathic. Because of this special property, Folch extraction ($\text{CHCl}_3/\text{MeOH}$) was used instead of ethyl acetate to extract lipid radical spin adducts. A larger amount of the Folch solvent compared to E.A. extraction was needed to be able to extract all cell lipids and interrupt the lipid peroxidation cycle.

We used two different cell lines for our experiments: K-562 cells are a human leukemia cell line that grows in suspension, while MCF-7 cells are a human breast carcinoma cell line that are adherent. Consistent with our DHA study, more information on the lipid-radical profile of cell membrane and LDL oxidations resulted upon extraction of spin adducts.

Lipid Peroxidation in K-562 Cells

EPR study in Cell Suspension

To induce lipid peroxidation in K-562 cells, we used singlet oxygen ($^1\text{O}_2$) as a tool. Singlet oxygen was produced by Photofrin, a photosensitizer used in photodynamic treatment of cancer. Upon light exposure, Photofrin produces $^1\text{O}_2$ that reacts with double bonds of unsaturated lipids, forming lipid hydroperoxides (LOOH) through a non-radical mechanism (Scheme 5). Radical chain reactions from these LOOHs can be initiated by ferrous iron (Scheme 5). The oxidizability of cells can be increased by enrichment of cell



Scheme 5. Proposed mechanism of Photofrin-mediated cellular lipid peroxidation.

membranes with PUFAs [Wagner BA, 1994]. PUFA such as DHA, can be added to the growth medium of the cells. After 48 h, most of the PUFAs are incorporated into the lipids of cell membranes.

Using the spin trap DEPMPO, we found weak EPR signals when Photofrin, light, or ferrous iron was absent, Figure 24 A-C. After K-562 cells were exposed to Photofrin/light for 5 min when Fe^{2+} was added, a burst of radical formation resulted, Figure 24 D. The radical reactions were detectable for 10 min in the dark after addition of Fe^{2+} (data not shown). These results show that the oxidizability of the cell membrane is greatly enhanced by Photofrin-light treatment *via* a Type II pathway.

Introduction of ferrous iron to the accumulated LOOHs in cell membranes will initiate a burst of radical formation *via* a Fenton-type reaction (reaction 4), which then propagates the radical events leading to cell damage and death. As seen in Figure 24, ferrous iron plays a key role in the initiation of the free radical-mediated oxidation of cell membranes.

Figure 24E-G shows time-dependent EPR spectra of DMPO adducts observed in Photofrin treated K-562 cells with continuous light exposure. Consistent with the DHA studies, we see that EPR analysis of cell membrane oxidation is limited because of the very short lifetimes of most spin adducts. Compared to the DHA study (Figure 9), far fewer radical adducts are detected in the cell system. For example, instead of four species in Figure 9A (DHA system), only two species are observed in Figure 24 (K-562). Those are the species with $a^{\text{N}} \approx 13.6 \text{ G}$, $a^{\text{H}} \approx 10.4 \text{ G}$ and $a^{\text{N}} \approx 12.9 \text{ G}$, $a^{\text{H}} \approx 6.95 \text{ G}$, 1.9 G . However, using our extraction technique, more radicals could be detected in K-562 cells.

EPR-Extraction and K-562 Oxidation

Figure 25 shows the EPR-extraction results of K-562 cells subjected to Photofrin/light and Fe^{2+} . After extraction, the lipid chain radicals are observed in the

Figure 24. EPR spectra of DEPMPO/L_d• (A-D) and DMPO/L_d• (E-G) formed from Photofrin-mediated membrane lipid peroxidation in K-562 cells. The spectra are representative of at least three different experiments.

- A: EPR spectrum of DEPMPO/L_d• from oxidation of K-562 cells (2×10^7 cells/mL) pre-treated with 9 $\mu\text{g/mL}$ Photofrin (45 min) and light (180 W/m^2 , 5 min). The K-562 cells were enriched with DHA; cell peroxidation was detected in the presence of 150 mM DMPO, 250 μM O₂, but, absent of Fe²⁺;
- B: Sample A without Photofrin treatment, oxidation was initiated by addition of 100 μM Fe²⁺;
- C: Sample A without light exposure, oxidation was initiated by addition of 100 μM Fe²⁺;
- D: Sample A without addition of 100 μM Fe²⁺;
- E: EPR spectrum of DMPO/L_d• from oxidation of K-562 cells (2×10^7 cells/mL) pre-treated with 9 $\mu\text{g/mL}$ Photofrin (45 min) and light (180 W/m^2 , 1 min). The K-562 cells were enriched with DHA; cell peroxidation was initiated by addition 100 μM Fe²⁺ in the presence of 250 μM O₂, 150 mM DMPO;
- F: Sample E, but 5 min of light exposure;
- G: Sample E, but 20 min light exposure.

A. K-562, light/ Fe^{2+}



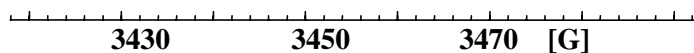
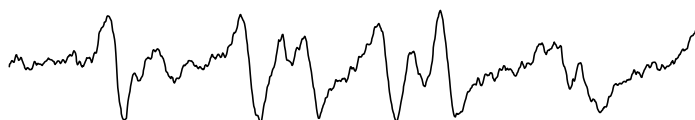
B. K-562, Photofrin/dark/ Fe^{2+}



C. K-562, Photofrin/light



D. K-562, Photofrin/light/ Fe^{2+}



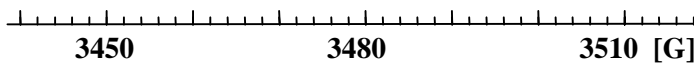
E. K-562, Photofrin/light, 1 min after Fe^{2+}



F. K-562, Photofrin/light, 5 min after Fe^{2+}



G. K-562, Photofrin/light, 20 min after Fe^{2+}



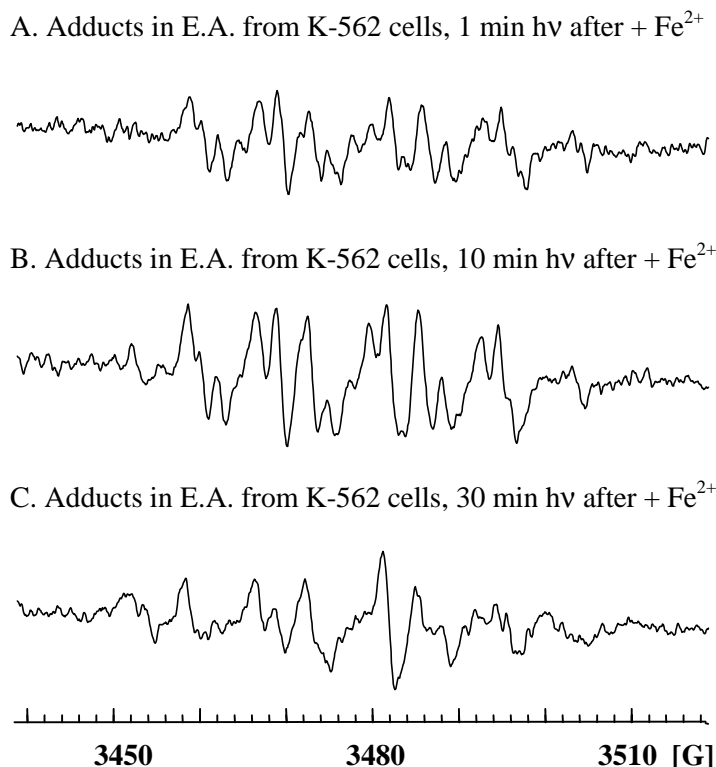


Figure 25. Lipid radicals can be trapped by DMPO from intact K-562 cells using the combination of EPR and Folch extraction. DHA-modified K-562 cells (5×10^6 cells/mL) were incubated with $6 \mu\text{g/mL}$ Photofrin followed by a 10 min exposure to visible light (100 W/m^2). This introduces LOOH into cell membranes *via* a non-radical mechanism. With $250 \mu\text{M}$ initial $[\text{O}_2]$, 150 mM DMPO, $110 \mu\text{M}$ DTPA and $100 \mu\text{M}$ Fe²⁺ were introduced to initiate free radical lipid peroxidation. All spectra are from 180 signal-averaged scans collected over a total of 30 min and are representative of at least three different experiments.

- A: EPR spectrum from the organic phase in E.A. after Folch extraction of sample: K-562 cell suspension described above, but cell sample received an additional 1 min light expose after introduction of Fe²⁺. The principal species are assigned as: DMPO/LOO[•] ($a^{\text{N}} \approx 12.9 \text{ G}$, $a^{\text{H}} \approx 6.95 \text{ G}$, 1.9 G); DMPO/LO[•] ($a^{\text{N}} \approx 13.6 \text{ G}$, $a^{\text{H}} \approx 10.4 \text{ G}$); and DMPO/OL[•] or DMPO/L[•] ($a^{\text{N}} \approx 13.8 \text{ G}$, $a^{\text{H}} \approx 22.7 \text{ G}$);
- B: Same as A, but extraction was applied at 10 min light expose after introduction of Fe²⁺;
- C: Same as A, but extraction was applied at 30 min light expose after introduction of Fe²⁺.

organic phase. Because radical adducts were stabilized by extraction, signal averaging could be performed for a longer time which resulted in good spectra. Different radical species with varying intensity could be observed in the EPR spectra at various extraction times. Two major EPR detectable species were found in E.A. with $a^N \approx 13.6$ G, $a^H \approx 10.4$ G; and $a^N \approx 12.9$ G, $a^H \approx 6.95$ G, 1.9 G. Species ($a^N \approx 13.6$ G, $a^H \approx 10.4$ G) in the E.A. phase is consistent with the long-chain lipid alkoxyl radical adduct DMPO/LO \bullet from the DHA studies (Figure 13); and the other species ($a^N \approx 12.9$ G, $a^H \approx 6.95$ G, 1.9 G) is consistent with the DMPO/OLOO \bullet from the DHA studies (Figure 13).

The 1:2:2:1 EPR signal ($a^N \approx a^H \approx 14.8$ G) in Figure 24 E, can also be observed in a Photofrin control (no cells) experiment upon light exposure. We observed this radical adduct in the DHA system and identified it as DMPO/ \bullet OH. Because this species was not observed in the E.A. phase after extraction it can not be a long chain lipid radical species, such as DMPO/LO \bullet or DMPO/OLOO \bullet (data not shown).

Compared to the DHA study, a much longer time for phase separation (16-20 h) was used for cell experiments to extract the lipid component from cells. After this longer time, the radical adducts in organic phase are then measured by EPR; but radical adducts in the aqueous phase are no longer observable. Thus, only information about radicals in the organic phase, *e.g.* the lipid-chain radical adducts, is available.

Summary of K-562 Cell Study

In the EPR study of Photofrin-light treated K-562 cells, we have shown that: (1) cell membranes undergo lipid peroxidation to produce lipid-derived radicals; LOOHs can accumulate in cell membranes due to Type II pathway from the Photofrin-light treatment and thus increase the oxidizability of the cells; (2) iron plays a vital role in initiation of cell membrane oxidation *via* LOOH to form LO \bullet , thereby driving the lipid radical reaction cycle; (3) Folch extraction can improve EPR spin trapping by stabilizing

lipid-chain radical spin adducts. Two lipid-chain radicals were observed in the organic phase. We propose that they are OLOO[•] and LO[•] radicals.

This study shows that EPR-extraction opens the door for studying radical events in cell membrane oxidation. In addition, it will help to shed light on other complex biological free radical oxidations where many radical events are involved that can compete with spin trapping reactions and destroy spin adducts. We propose that this method has great potential for research in biological systems with EPR, and that this extraction technique will soon be adapted to study radical formation from different targets, (e.g. DNA, and proteins), in living systems (e.g. different organs).

Lipid Peroxidation in MCF-7 Cells

Due to the current limitation of EPR methodology, direct real time studies of intact cells, for all practical purposes, is limited to suspension cells. This is due to the difficulty of transferring intact adherent cells into the EPR flat cells.

EPR-Extraction and MCF-7 Cell Oxidation

Before the development of our extraction technique, it was extremely difficult to detect radical formation in adherent cells by EPR. In contrast to suspension cells, such as K-562 cells, the adherent cells could not be easily transferred into an EPR flat cell. However, with our unique extraction technique, we should be able to detect lipid-derived radicals as has been done with K-562 cells. To test this proposal, we induced lipid peroxidation in MCF-7 cells using Photofrin as a tool to produce singlet oxygen.

The proposed mechanism of Photofrin-mediated cell membrane radical oxidation is that LOOHs are formed and accumulate in cell membranes *via* a non-radical mechanism (Scheme 5). Upon addition of ferrous iron, these LOOH molecules undergo

radical chain reactions. Phospholipid hydroperoxide glutathione peroxidase (PhGPx) is an antioxidant enzyme that can remove LOOH: [Ursini F, 1985; 1985; Thomas JP, 1990]



Thus, it can interfere with Photofrin/light treatment by reducing the level LOOH formed during light exposure. We hypothesize that overexpression of PhGPx will remove the LOOH, thereby decreasing radical formation after PDT with Photofrin.

We used MCF-7 cells (parental, wild type cells) and MCF-7 cells that overexpress the mitochondrial form of PhGPx (3-fold to 8- fold overexpression) to test our hypothesis [Wang H, 1999]. MCF-7 cells were incubated with 6 $\mu\text{g/mL}$ Photofrin for 24 h in full medium and exposed to light in PBS for 5 min. Cells were then incubated for 6 h in the dark at 37°C in full medium. We incubated these cells for 6 h in the dark to give PhGPx the time needed to remove the LOOHs accumulated in the membrane. The medium was replaced with PBS and DMPO (150 mM) and Fe^{2+} (100 μM) were added. As in our EPR-extraction study with K-562 cells, radical-adducts were only observed in the organic phase, *e.g.* the lipid-chain spin adducts, Figure 26.

We observed a DMPO/LO \cdot spin adduct ($a^{\text{N}} \approx 13.5 \text{ G}$, $a^{\text{H}} \approx 10.2 \text{ G}$) in the organic phase of the parental cells and transfected cells. Small amounts of a DMPO/OLOO \cdot (marked by * in Figure 26) spin adduct was detected in the wild type and the neo type. From three independent experiments we found that both Wt and Neo cell lines show increased radical formation compared to PhGPx-overexpression cells. As expected, overexpression of PhGPx correlates indirectly with spin adduct formation; the higher the PhGPx activity, the lower the amount of spin adducts observed (Figure 27). For example, PhGPx51 the clone with the highest level of PhGPx (8.4-fold increase) inhibits DMPO-adduct formation completely compared to Wt and Neo.

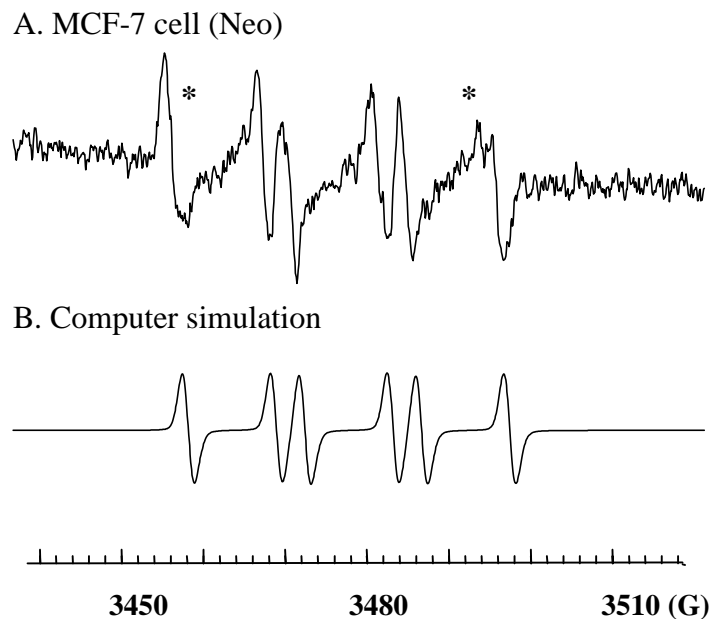


Figure 26. Lipid-derived free radicals are generated from MCF-7 cells following Photofrin/light treatment. MCF-7 cells were treated with 6 $\mu\text{g/mL}$ Photofrin for 24 h, cells were exposed to light for 5 min (5 J/m^2). Cells were then incubated in the dark for 6 h. After Photofrin/light treatment, cells were incubated with 150 mM DMPO and 100 μM ferrous iron for 5 min. The lipids and lipid radicals were extracted with $\text{CHCl}_3\text{:MeOH}$ (2:1, v/v). The chloroform layer was dried under argon, and redissolved in 500 μL degassed ethyl acetate. The ethyl acetate was immediately transferred to an EPR flat cell and EPR scans started. DMPO/ LO^\bullet spin adducts was mainly observed. This spectrum is representative of three different experiments.

A: Wt cells with light treatment. The asterisk represents the position of a potential DMPO/ OLOO^\bullet spin adduct. The similar spectra, but with different intensities, were observed from all the cell lines examined.

B: Computer simulation of A. $a^{\text{N}} \approx 13.6 \text{ G}$, $a^{\text{H}} \approx 10.4 \text{ G}$

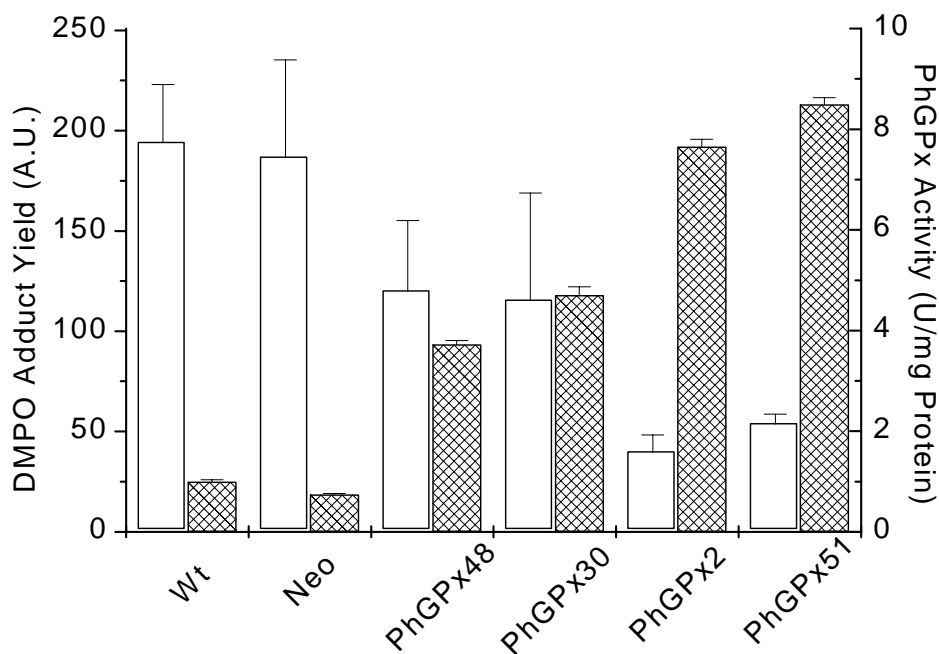


Figure 27. Radical yield from MCF-7 cells and their L-PhGPx transfectants. The open bar represents DMPO adduct yield; and checked bar represents PhGPx activity. A yield of 70 A.U. was considered to be background noise-level. Cells were pretreated with 6 $\mu\text{g}/\text{mL}$ Photofrin for 24 h, and exposed to light for 5 min. Cells were then incubated in full media for 6 h. After that, cells were washed and incubated with 100 mM DMPO and 100 μM ferrous iron for 5 min in metal-free PBS at room temperature. The lipids and lipid radicals were extracted with chloroform:methanol (2:1, v/v). The chloroform layer was dried under argon, and redissolved in 500 μL degassed ethyl acetate. The ethyl acetate was immediately transferred to an EPR flat cell and EPR scans started. The DMPO/ LO^\bullet spin adduct was observed ($a^{\text{N}} \approx 15.2 \text{ G}$, $a^{\text{H}} \approx 10.2 \text{ G}$). Data are representative of three experiments. Error bar represents standard derivation.

Summary of MCF-7 Cell Study

These experiments show that our extraction technique can be used for adherent cells. This is first time that lipid-derived oxygen-centered radical formation could be observed from adherent cells.

Based on this experimental evidence, we conclude that: (1) lipid peroxidation plays an important role in PDT-induced photo-toxicity; (2) PhGPx provides significant protection in cells from PDT photo-oxidation, (3) EPR-extraction is a good tool for detecting lipid radicals from adherent cells.

Low-Density Lipoprotein Oxidation

Low-density lipoproteins, LDL, is an approximately spherical molecule. In humans, each LDL molecule contains about 600 molecules of cholesterol, 1600 molecules of cholesterol ester, and 170 molecules of triglyceride within a hydrophobic core that is wrapped in a monolayer of 700 phospholipid molecules [Halliwell B, 1999]. Due to the high content of oxidizable compounds, such as phospholipids and cholesterol esters, LDL has a high potential to undergo lipid peroxidation producing lipid free radicals. The oxidation of LDL in vessel walls is thought to be an important mechanistic events of atherosclerosis [Steinberg, D , 1989]. Until now, lipid chain radicals in LDL oxidation were not successfully detected by EPR techniques [Kalyanaraman B, 1990]. We have applied the Folch extraction to detect lipid-derived radicals during copper-mediated LDL oxidation. Our new extraction technique will help in the understanding of the radical processes in the mechanism of oxidation of LDL.

EPR-Extraction and LDL Oxidation

A suspension of LDL in phosphate buffer was treated with DMPO and Cu^{2+} , and then examined by EPR with and without Folch extraction. LDL produces EPR detectable

spin adducts in both the PB-LDL suspension and the organic phase, Figure 28. Due to the way the experiment had to be designed, radical adducts in the aqueous phase were either oxidized or reduced *via* iron, thus not detectable. In the PB-LDL suspension, there is only a very weak EPR signal with a 1:2:2:1 intensity pattern observed 10-15 min after Cu^{2+} was introduced. Twenty minutes after Cu^{2+} was introduced, no EPR signal was detected. However, Folch extraction of the oxidizing LDL system stabilized the radical adducts and thus EPR signals could be observed 1, 10, and 20 min after addition of Cu^{2+} . In contrast to the DHA study, the most intense EPR signals were observed late in the oxidation, 10 min after Cu^{2+} addition. Two radical adducts were observed in the ethyl acetate phase and identified as LO^\bullet ($a^{\text{N}} \approx 13.6$ G, $a^{\text{H}} \approx 10.4$ G) and LOO^\bullet ($a^{\text{N}} \approx 12.9$ G, $a^{\text{H}} \approx 6.95$ G, 1.9 G). These data demonstrate that the extraction technique is also valuable in studying lipid peroxidation in biological molecules such as LDL.

Summary of LDL Oxidation

We conclude that EPR spin trapping coupled with organic extraction can overcome some of the disadvantages of EPR detection of lipid-derived radicals in biological systems, thereby providing new strategies for studying the free radical events of biological lipid peroxidation. The extraction technique can be easily adapted to study radical production of the lipid-related component of oxidation in biological materials such as suspension cells, adherent cells, and perhaps tissue that can not be investigated by normal EPR spin trapping approaches. The longer lifetime of spin adducts post-extraction provides an opportunity for identifying the structure of radicals *via* EPR, HPLC and MS. Furthermore, by performing extraction at specific time points, the profile of all lipid-derived radicals can be correlated to cytotoxicity. This will be a leap forward in our understanding of the free radical mechanism of lipid peroxidation in biological systems.

Figure 28. Lipid radical production from LDL oxidation. A typical incubation for an EPR experiment consisted of 2.2 mg/mL of LDL, 100 mM DMPO, and 100 μM Cu^{2+} in PB. To analyze spin adducts in PB-LDL suspension, the incubation mixture (500 μL) with 250 μM initial $[\text{O}_2]$, was transferred into EPR flat cell for EPR measurement. For analysis of spin adducts in organic extracts, the incubation mixture (500 μL) was extracted using the Folch method before EPR measurement. A, C, and E are spectra from 3 signal-averaged scans collected over a total of 2 min; B, D, and F are spectra from 60 signal-averaged scans collected over a total of 40 min. All spectra are representative of three different experiments.

A: EPR spectrum of the PB-LDL suspension oxidized 1 min after introduction of Cu^{2+} ;

B: EPR spectrum of the organic phase of sample A post-extraction;

C: Sample A; but 10 min after introduction of Cu^{2+} ;

D: EPR spectrum of the organic phase of sample C post-extraction (DMPO/LOO \cdot : $a^{\text{N}} \approx 12.9$ G, $a^{\text{H}} \approx 6.95$ G, 1.9 G; DMPO/LO \cdot : $a^{\text{N}} \approx 13.6$ G, $a^{\text{H}} \approx 10.4$ G);

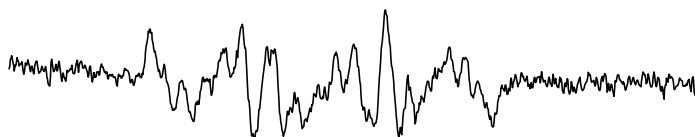
E: Sample A; but 20 min after introduction of Cu^{2+} ;

F: EPR spectrum of the organic phase of sample E post-extraction.

A. PBS-LDL suspension, 1 min after + Cu²⁺



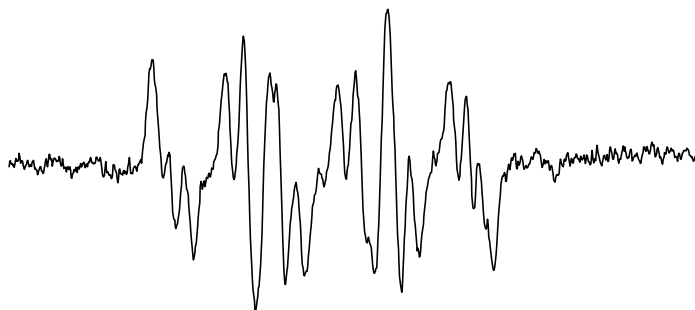
B. E.A. phase after Folch extraction of A



C. PBS-LDL suspension, 10 min after + Cu²⁺



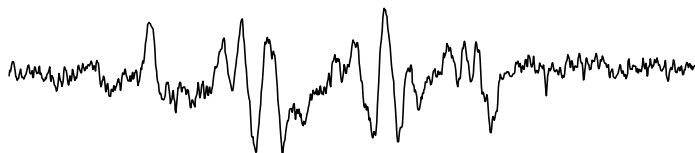
D. E.A. phase after Folch extraction of C



E. PBS-LDL suspension, 20 min after + Cu²⁺



F. E.A. phase after Folch extraction of E



3450

3480

3510 (G)

CHAPTER V

FUTURE DIRECTIONS

When using spin trapping, the structure and identification of the radicals observed has been based largely on EPR hyperfine coupling constants of the spin adducts. However, similar hyperfine splitting constants are often observed for different radical adducts, which makes identification of radical adducts difficult. In this research program, we have used extraction techniques to enhance EPR spin trapping so we can obtain more comprehensive information on the radical adducts. Extraction adds to our knowledge of the spin adducts because we learn something of their hydrophilic or hydrophobic properties in addition to their EPR hyperfine splitting constants in different solvents. Our improved EPR-extraction technique as developed, for the first time gives information for the determination of lipid chain radicals produced from PUFA, cells, and LDL.

In addition to EPR, other powerful tools to identify radical adducts are HPLC and MS. There are several reports that have used HPLC/EPR and LC/MS to determine the detailed structure of POBN radical adducts from lipid peroxidation, such as soybean lipoxygenase-mediated PUFA oxidation [Iwahashi H, 1990; 1991; 1991]. However, as mentioned above, POBN traps mainly radicals derived from the β -scission pathway, which may only be a minor pathway for lipid peroxidation. There are few reports on HPLC and MS studies of DMPO spin adducts, and they are only limited to simple chemistry models. Due to the big improvements in stability of these adducts by EPR-extraction, the significance of lipid-oxygen-centered radicals in lipid peroxidation can

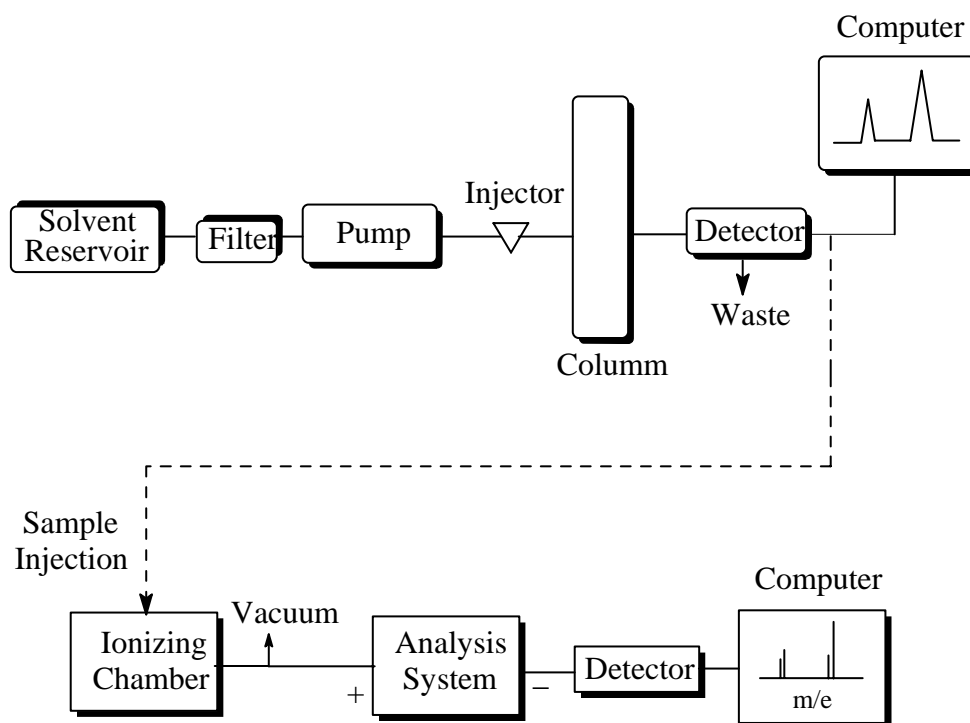
now be studied by HPLC/MS. Thus, our goal is to use HPLC and MS to identify the lipid-chain radicals and correlate them to cytotoxicity.

HPLC and MS

High performance liquid chromatography (HPLC) is a chromatographic method in which a mobile solvent liquid phase is forced under controlled high pressure through a relatively narrow column containing a stationary phase (See Scheme 6). An essential component of the HPLC is a solvent delivery system, which comprises solvent reservoirs, filters, and a pump. The solvent is delivered at a set flow rate under pressures of 2500-3000 psi. The second component is the injection system. This is used to introduce sample to the column without releasing the pressure. The column is a polished stainless steel tube and packed with a micro-particle material. Different columns are usually required for different analyses in order to achieve reproducible separation of different compounds. Finally, a detector is used to identify and quantify each component of the sample.

Mass spectrometry (MS) is a powerful analytical detection method that can supply qualitative and quantitative data [Iwahshi H, 1996], not readily obtained by other means. It can provide the molecular weight, the empirical formula, and often the complete structure of an unknown compound. A schematic diagram of MS is shown in Scheme 6.

The combination of mass spectrometry and HPLC is especially effective to further our research goals. A fraction of the column effluent would be sent directly to the inlet of the mass spectrometer, and yield a mass spectrum of the substance. When the mass spectrum and the retention characteristics both agree with those of a known material, identification is virtually certain. Furthermore, provided that operating



Scheme 6. The schematic diagram of HPLC and MS.

conditions, such as temperature and flow rate are carefully reproduced, the retention volume for a given substance will also be reproducible and can serve as a means of identification. The identity of the components of a mixture can usually be established with greater certainty by comparison with known materials and by the use of two or more kinds of liquid stationary phase.

The major difficulty in the use of HPLC and MS in conjunction with EPR and spin trapping is the stability of the spin adducts. The extraction approach we have devised greatly increases the stability of the spin adducts of DMPO and DEPMPO that arise during lipid peroxidation. With this tool in hand we can now use the HPLC and MS approaches to study radical formation during lipid peroxidation. Previously, this has only been possible for the carbon-centered radical adducts of POBN. Our extraction technique has opened a new window of opportunity to study free radical-mediated lipid peroxidation in biology.

REFERENCES

- Bennett, J. E. J. A kinetic study of the self-reaction of prop-2-peroxyl radicals in solution using ultraviolet absorption spectroscopy. *Chem. Soc. Faraday Trans. I.* 83: 1805-18013; 1987.
- Buettner, G. R. Spin trapping: ESR parameters of spin adducts. *Free Radic. Biol. Med.* 3: 259-303; 1987.
- Buettner, G. R. In the absence of catalytic metals ascorbate does not autoxidize at pH 7: ascorbate as a test for catalytic metals. *J. Biochem. Biophys. Meth.* 16: 27-40; 1988.
- Buettner, G. R. On the reaction of superoxide with DMPO/•OOH. *Free Rad. Res. Comm.* 10: 11-15; 1990.
- Buettner, G. R.; Kelley, E. E.; Burns, C. P. Membrane lipid free radicals produced from L1210 murine leukemia cells by Photofrin Photosensitization: An EPR spin trapping study. *Cancer Res.* 53: 3670-3673; 1993.
- Buettner, G. R. Free radical chemistry: the pecking order and more. Sunrise Free Radical School Lecture. The annual meeting of the Oxygen Society, Pasadena, CA, 1995.
- Burns, C. P.; Haugstad, B. N.; Mossman, C. J.; North, J. A.; Ingraham, L. M. Membrane lipid alteration: effect on cellular uptake of mitoxantrone. *Lipids.* 23: 393-397; 1988.
- Burns, C. P.; Wagner, B. A. Heightened susceptibility of fish oil polyunsaturate-enriched neoplastic cells to enriched neoplastic cells to ethane generation during lipid peroxidation. *J. Lipid Res.* 32: 79-87; 1991.
- Chamulitrat, W.; Hughes, M. F.; Eling, T. E.; Mason, R. P. Superoxide and peroxy radical generation from the reduction of polyunsaturated fatty acid hydroperoxides by soybean lipoxygenase. *Arch. Biochem. Biophys.* 290: 153-159; 1991.
- Chamulitrat, W.; Iwahashi, H.; Kelman, D. J.; Mason, R. P. Evidence against the 1:2:2:1 quartet DMPO spectrum as the radical adduct of the lipid alkoxyl radical. *Arch. Biochem. Biophys.* 296: 645-649; 1992.

- Davies, M. J. Detection of peroxy and alkoxy radicals produced by reaction of hydroperoxides with heme-proteins by electron spin resonance spectroscopy. *Biochim. Biophys. Acta.* 964: 28-35; 1988.
- Davies, M. J.; Slater, T. F. Studies on the metal-ion and lipoxygenase-catalyzed breakdown of hydroperoxides using electron-spin-resonance spectroscopy. *Biochem. J.* 245: 167-173; 1987.
- Dikalov, S. I.; Mason, R. P. Reassignment of organic peroxy radical adducts. *Free Radic. Biol. Med.* 27: 864-872; 1999.
- Feix J. B. Kalyanaraman B. Spin trapping of lipid-derived radicals in liposomes. *Biochim. Biophys. Acta.* 992: 230-235, 1989.
- Frejaville, C.; Karoui, H.; Tuccio, B.; Le Moigne, F.; Culcasi, M.; Pietri, S.; Lauricella, R.; Tordo, P. 5-(diethoxyphosphoryl)-1-methyl-1-pyrroline-*N*-oxide: a new efficient phosphorylated nitron for the in vitro and in vivo spin trapping of oxygen-centered radicals. *J. Med. Chem.* 38: 258-265, 1995.
- Gardner, H. W. Oxygen radical chemistry of polyunsaturated fatty acids. *Free Radic. Biol. Med.* 7: 65-86; 1989.
- Girotti, A. W. Mechanisms of lipid peroxidation. *Free Radic. Biol. Med.* 1: 87-95; 1985.
- Guffy, M. M.; North, J. A.; Burns, C. P. Effect of cellular fatty acid alteration on adriamycin sensitivity in cultured L1210 leukemia cells. *Cancer Res.* 44: 1863-1866; 1984.
- Hanna, P. M.; Chamulitrat, W.; Mason, R. P. When are metal ion-dependent hydroxyl and alkoxy radical adducts of 5, 5-dimethyl-1-pyrroline *N*-oxide artifacts? *Arch. Biochem. Biophys.* 296: 640-644; 1992.
- Hasegawa, K.; Patterson, L. K. Pulse radiolysis studies in model lipid systems: formation and behavior of peroxy radicals in fatty acids. *Photochem. Photobiol.* 28: 817-823; 1978.
- Halliwell, B.; Gutteridge, J. M. C. (1999) *Free Radicals in Biology and Medicine.* Oxford University Press Inc. New York.
- Howard, J. A.; Tait, J. C. Electron paramagnetic resonance spectra of the *tert*-butylperoxy and *tert*-butoxy adducts to phenyl *tert*-butyl nitron and 2-methyl-2-nitrosopropane. Oxygen-17 hyperfine coupling constants. *Can. J. Chem.* 56: 176-178; 1978.

Iwahashi, H.; Albro, P. W.; McGown, S. R.; Tomer, K. B.; Mason, R. P. Isolation and identification of alpha-(4-pyridyl-1-oxide)-N-tert-butyl nitron radical adducts formed by the decomposition of the hydroperoxides of linoleic acid, linolenic acid, and arachidonic acid by soybean lipoxygenase. *Arch. Biochem. Biophys.* 285: 172-80; 1991.

Iwahashi, H.; Parker, C. E.; Mason, R. P.; Tomer, K. B. Radical adducts of nitrosobenzene and 2-methyl-2-nitrosopropane with 12,13-epoxylinoleic acid radical, 12,13-epoxylinolenic acid radical and 14,15-epoxyarachidonic acid radical. Identification by HPLC-EPR and liquid chromatography-thermospray-M.S. *Biochemical J.* 276: 447-53; 1991.

Iwahashi, H.; Parker, C. E.; Mason, R. P.; Tomer, K. B. Radical identification by liquid chromatography/thermospray mass spectrometry. *Rapid Commun. Mass Spect.* 4: 352-354; 1990.

Janzen, E. G.; Krygsmann, P. H.; Lindsay, D. A.; Haire, D. L. Detection of alkyl, alkoxy, and alkyperoxy radicals from the thermolysis of azobis (isobutyronitrile) by ESR/spin trapping. Evidence for double spin adducts from liquid-phase chromatography and mass spectroscopy. *J. Am. Chem. Soc.* 112: 8279-8284; 1990.

Jori, G. (1980) The molecular biology of photodynamic action. In Pratesi R. Succica (eds). *Lasers in Photomedicine and Photobiology*. Springer-Verlag, Berlin. pp58-66.

Kalyanaraman, B.; Mottley C; Mason, R. P. On the use of organic extraction in the spin-trapping technique as applied to biological systems. *J. Biochem. Biophys. Meth.* 9: 27-31; 1984.

Kalyanaraman, B.; Antholine, W. E.; Parthasarathy, S. Oxidation of low-density lipoprotein by Cu^{2+} and lipoxygenase: an electron spin resonance study. *Biochim. Biophys. Acta.* 1035: 286-92; 1990.

Kelley, E. E.; Buettner, G. R.; Burns, C. P. Production of lipid-derived free radicals in L1210 murine leukemia cells is an early event in the photodynamic action of Photofrin. *Photochem. Photobiol.* 64: 576-580; 1997.

Kocherginsky, N.; Swartz, H. M. Chemical reactivity of nitroxides. In: Kocherginsky, N.; Swartz, H. M., eds. *Nitroxide Spin Labels: Reactions in Biology and Chemistry*. Boca Raton, FL: CRC Press. 1995: 48-49.

Kotake, Y.; Reinke, L. A.; Tanigawa, T.; Koshida, H. Determination of the rate of superoxide generation from biological systems by spin trapping: use of rapid oxygen depletion to measure the decay rate of spin adducts. *Free Radic. Biol. Med.* 17: 215-223; 1994.

- Krainev, A. G.; Bigelow, D. J. Comparison of 2,2'-azobis (2-amidinopropane) hydrochloride (AAPH) and 2,2'-azobic (2, 4-dimethylvaleronitrile) (AMVN) as free radical initiators: a spin-trapping study. *J. Chem. Soc. Perkin Trans. 2.* 747-754; 1996.
- Krainev, A. G.; Williams, T. D.; Bigelow, D. J. Oxygen-centered spin adducts of 5,5-dimethyl-1-pyrroline *N*-oxide (DMPO) and 2H-imidazole 1-oxides. *J. Magn. Reson.* 111(B): 272-280; 1996.
- Li, A. S. W.; Cummings, K. B.; Roethling, H. P.; Buettner, G. R.; Chignell, C. F. A Spin Trapping Database Implemented on the IBM PC/AT. *J. Mag. Res.* 79: 140-142, 1988.
- Liu, K.J.; Miyake, M.; Panz ,T.; Swartz, H. Evaluation of DEPMPO as a spin trapping agent in biological systems. *Free Radic. Biol. Med.* 26: 714-21; 1999.
- Maiorino, M.; Roveri, A.; Ursini, F.; Gregolin C. Enzymatic determination of membrane lipid peroxidation. *Free Radic. Biol. Med.* 1: 203-7; 1985.
- Makino, K.; Hagiwara, T.; Hagi, A.; Nishi, M.; Murakami, A. Cautionary note for DMPO spin trapping in the presence of iron ion. *Biochem. Biophys. Res. Commun.* 172: 1073-1080; 1990.
- Marnett, L. J.; Wilcox, A. L. The Chemistry of lipid alkoxy radical and their role in metal-amplified lipid peroxidation. In: Rice-Evans, C.; Halliwell, B.; Lunt, G. G., eds. *Free Radicals and Oxidative Stress: Environment, Drugs and Food Additives.* Biochem. Soc. Symp. 61: 65-72; 1996.
- Mason, R. P.; Kalyanaraman, B.; Tainer B. E.; Eling, T. E. A carbon-centered free radical intermediate in the prostaglandin synthetase oxidation of arachidonic acid: spin trapping and oxygen uptake studies. *J. Biol. Chem.* 255: 5019-5022; 1980.
- Qian, S. Y.; Buettner, G. R. Iron and dioxygen chemistry is an important route to initiation of biological free radical oxidations: an electron paramagnetic resonance spin trapping study. *Free Radic. Biol. Med.* 26: 1447-1456; 1999.
- Rota, C.; Barr, D. P.; Martin, M. V.; Guengerich, F. P.; Tomasi, A.; Mason, R. P. Detection of free radicals produced from the reaction of cytochrome *P*-450 with linoleic acid hydroperoxide. *Biochem. J.* 328: 565-571; 1997.
- Roubaud, V.; Sankarapandi, S.; Kuppusamy P.; Tordo P.; Zweier, J. L. Quantitative measurement of superoxide generation using the spin trap 5-diethoxyphosphoryl-5-methyl-1-1pyrroline-*N*-oxide. *Anal. Biochem.* 247: 404-411, 1997.
- Roubaud, V.; Sankarapandi, S.; Kuppusamy, P.; Tordo, P.; Zweier, J. L. Quantitative measurement of superoxide generation and oxygen consumption from leukocytes using electron paramagnetic resonance spectroscopy. *Anal. Biochem.* 257: 201-207; 1998.

- Schafer, F. Q.; Buettner, G. R. Acidic pH amplifies iron-mediated lipid peroxidation in cells. *Free Radic. Biol. Med.* Submitted: 1999.
- Schaich, K. M.; Borg, D. C. Solvent effects in the spin trapping of lipid oxyl radicals. *Free Rad. Res. Comm.* 9: 267-278; 1990.
- Steinberg, D.; Parthasarathy, S.; Carew, T. E.; Khoo, J. C.; Witztum, J. L. Beyond cholesterol: modifications of low-density lipoprotein that increase its atherogenicity. *N. Engl. J. Med.* 320: 915-924; 1989.
- Thomas, J. P.; Maiorino, M.; Ursini, F.; Girotti, A. W. Protective action of phospholipid hydroperoxide glutathione peroxidase against membrane-damaging lipid peroxidation. In situ reduction of phospholipid and cholesterol hydroperoxides. *J. Biol. Chem.* 265: 454-61; 1990.
- Trudell, J. R. Ethyl acetate extraction of spin-trapped free radicals: a reevaluation. *Free Radic. Biol. Med.* 3: 133-136; 1987.
- Tuccio, B.; Lauricella, R.; Bouteiller, J. C.; Tordo, P. *J. Chem. Soc. Perkin Trans.* 295-298. 1995.
- Ursini, F.; Maiorino, M.; Gregolin, C. The selenoenzyme phospholipid hydroperoxide glutathione peroxidase. *Biochim. Biophys. Acta.* 839: 62-70; 1985.
- Wagner, B. A.; Buettner, G. R.; Burns, C. P. Free radical-mediated lipid peroxidation in cells: oxidizability is a function of cell lipid *bis*-allylic hydrogen content. *Biochemistry.* 33: 4449-4453; 1994.
- Wagner, B. A.; Buettner, G. R.; Burns, C. P. Increased generation of lipid-derived and ascorbate free radicals by L1210 cells exposed to the ether lipid edelfosine. *Cancer Res.* 53: 711-713; 1993.
- Wagner, B. A.; Buettner, G. R.; Oberley, L. W.; Burns, C. P. Sensitivity of K-562 and HL60 cells to edelfosin, a ether lipid drug, correlates with production of active oxygen species. *Cancer Res.* 58: 2809-2816; 1998.
- Wang, H.; Buettner G. R.; Oberley L. W. Overexpression of human PhGPx in human breast cancer cells (MCF-7): Effects on Photofrin photosensitization. *Photochem. Photobiol.* 69: 36S; 1999.
- Wilcox, A. L.; Marnett, L. J. Polyunsaturated fatty acid alkoxy radicals exist as carbon-centered epoxyallylic radicals: a key step in hydroperoxide-amplified lipid peroxidation. *Chem. Res. Toxicol.* 6: 413-416; 1993.

Wilkinson, F.; Brummer, J. G. Rate constants for the decay and reactions of the lowest electronically excited singlet state of molecular oxygen in solution. *J. Phys. Chem. Ref. Data.* 10: 809-999; 1981.